Running as fast as it can:

How spiking dynamics form object groupings in the laminar circuits of visual cortex

Jasmin Léveillé, Massimiliano Versace, and Stephen Grossberg

Department of Cognitive and Neural Systems
Center for Adaptive Systems
and
Center of Excellence for Learning in Education, Science, and Technology
Boston University, 677 Beacon Street, Boston, MA 02215, USA

Running title: grouping by spiking laminar cortical circuits

Submitted: July 6, 2009
Revised: January 5, 2010

Technical Report CAS/CNS-0009-010

In press: *Journal of Computational Neuroscience*

All correspondence should be addressed to:
Professor Stephen Grossberg
Department of Cognitive and Neural Systems
Boston University
677 Beacon Street
Boston, MA 02215
Phone: 617-353-7858/7
Fax: 617-353-7755
Email:steve@bu.edu

Abstract

How spiking neurons cooperate to control behavioral processes is a fundamental problem in computational neuroscience. Such cooperative dynamics are required during visual perception when spatially distributed image fragments are grouped into emergent boundary contours. Perceptual grouping is a challenge for spiking cells because its properties of collinear facilitation and analog sensitivity occur in response to binary spikes with irregular timing across many interacting cells. Some models have demonstrated spiking dynamics in recurrent laminar neocortical circuits, but not how perceptual grouping occurs. Other models have analyzed the fast speed of certain percepts in terms of a single feedforward sweep of activity, but cannot explain other percepts, such as illusory contours, wherein perceptual ambiguity can take hundreds of milliseconds to resolve by integrating multiple spikes over time. The current model reconciles fast feedforward with slower feedback processing, and binary spikes with analog network-level properties, in a laminar cortical network of spiking cells whose emergent properties quantitatively simulate parametric data from neurophysiological experiments, including the formation of illusory contours; the structure of non-classical visual receptive fields; and self-synchronizing gamma oscillations. These laminar dynamics shed new light on how the brain resolves local informational ambiguities through the use of properly designed nonlinear feedback spiking networks which run as fast as they can, given the amount of uncertainty in the data that they process.

Keywords: perceptual grouping, laminar cortical circuit, spiking neuron, visual cortex, gamma oscillations, illusory contour, bipole cell

1 Introduction: perceptual grouping in the laminar circuits of visual cortex

From Spikes to Behavior: The Challenge Posed by Perceptual Grouping. Although many neurons communicate in the brain using discrete spikes, there are surprisingly few studies that show how spiking neurons cooperate to control behavioral processes. Such cooperative dynamics are required during visual perception when spatially distributed image fragments are grouped into emergent boundary contours. Grouping of local image contrasts is an important step in the perceptual organization process that leads to the emergence of 3D object boundary representations. Such boundaries delimit object borders and surfaces, allowing the brain to build meaningful perceptual units in response to complex scenes, and thereby contributing to global form perception. While perceptual grouping has long been studied in psychology, and several models of perceptual grouping have been proposed, it remains necessary to fully characterize the mechanisms and functions in laminar cortical circuits whose cell communicate via spiking dynamics. In particular, although models have been introduced that begin to explain how spiking neurons within laminar circuits of visual cortex support certain perceptual and cognitive processes, spiking laminar models of perceptual grouping remain to be characterized.

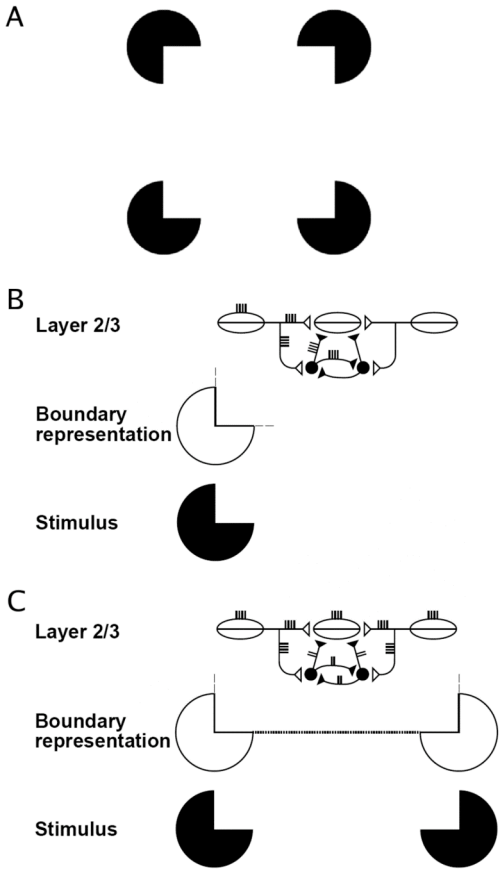

Fig. 1 Perceptual grouping by bipole cell interactions: (A) The four pac man figures induce the percept of a Kanizsa square whose sides are delimited by illusory contours. (B) Input from a single pac man is insufficient to induce illusory contours. (C) Input from a pair of collinear pac man edges creates an illusory contour by activating bipole cells at all positions between them.

Illusory contour stimuli illustrate the requirements that must be satisfied by an adequate grouping mechanism. Illusory contours show that perceptual boundaries are completed only in regions enclosed by properly aligned boundary inducers. As described in greater detail below, some models have demonstrated spiking dynamics in recurrent laminar neocortical circuits, but not how perceptual grouping occurs. Other models have analyzed the fast speed of certain percepts in terms of a single feedforward sweep of activity, but cannot explain other percepts, such as illusory contours, wherein perceptual ambiguity can take hundreds of milliseconds to resolve by integrating multiple spikes over time. The current model reconciles fast feedforward with slower feedback processing, and binary spikes with analog network-level properties, in a laminar cortical network of spiking cells whose emergent properties quantitatively simulate parametric data from neurophysiological experiments, including the formation of illusory contours; the structure of non-classical visual receptive fields; and self-synchronizing gamma oscillations. These laminar dynamics shed new light on how the brain resolves local informational ambiguities through the use of properly designed nonlinear feedback networks that run as fast as they can, given the amount of uncertainty in the data that they process, and automatically slow down processing to use internal feedback processes to resolve informational ambiguities before speeding up again. In other words, the brain is designed in many situations to trade informational uncertainty against speed.

A classic example of an illusory contour is shown in Figure 1A. Here, a Kanizsa square stimulus with four pacmen inducers leads to the percept of a bright square bounded by illusory contours. A parsimonious explanation is that neural signals corresponding to almost collinear pairs of edge inducers complete over the gap that separates them, as reported in the neurophysiological data of von der Heydt et al. (1984) and Peterhans and von der Heydt (1989), among others (see Table 1). A key problem to solve is why illusory contours do not propagate from a single image inducer. Were this possible, then every dot in an image could propagate uncontrollably in all directions to fill the image percept. This does not occur because *inward* boundary completion between pairs or greater numbers of inducers, on opposite sides of a target cell, occurs without causing uncontrollable *outward* boundary propagation from a single inducer. This has been called the *bipole grouping property* in the Boundary Contour System, or BCS, model of perceptual grouping and boundary completion that was introduced by Grossberg and his colleagues (e.g., Cohen and Grossberg 1984; Grossberg 1984; Grossberg and Mingolla 1985a, 1985b). Psychophysical experiments on association fields (Field et al. 1993) and contour interpolation (Kellman and Shipley 1992), among others, have supported the bipole grouping concept.

The more recent 3D LAMINART model has refined the analysis of bipole grouping by predicting how it takes place in laminar cortical circuits, and has thereby explained much larger psychophysical and neurobiological data bases that depend upon perceptual grouping, including properties of cortical development, perceptual learning, attention, 3D vision, figure-ground separation, and perceptual bistability, including Necker cube bistability and binocular rivalry (e.g., Cao and Grossberg 2005; Fang and Grossberg 2009; Grossberg and Raizada 2000; Grossberg and Swaminathan 2004; Grossberg and Williamson 2001; Grossberg and Yazdanbakhsh 2005; Grossberg et al. 2008; Yazdanbakhsh and Grossberg 2004). However, neurons in these laminar cortical models use rate coding, rather than spikes, to represent intercellular signals.

Table 1 Model connections and supporting anatomical data.

Model connection	Functional interpretation	Selected references
LGN → 4	Strong LGN input	Blasdel and Lund (1983); Ferster et al. (1996); Thomson et al. (2003)
4 → 2/3 pyramidals	Feedforward stimuli with bottom-up support	Fitzpatrick et al. (1985); Callaway and Wiser (1996); Shmuel et al. (2005)
V1 2/3 pyr. → 2/3 pyr.	Long-range collinear integration	Bosking et al. (1997); Schmidt et al. 1997); Chisum et al. (2003)
V2 2/3 pyr. → 2/3 pyr.	Long-range collinear integration	Levitt et al. (1994)
2/3 pyr. → 2/3 inhib. int.	Keep outward grouping subthreshold (bipole property)	McGuire et al. (1991); Hirsch and Gilbert (1991); Holmgren et al. (2003)
2/3 inhib. int. → 2/3 pyr.	Keep outward grouping subthreshold (bipole property)	Lund et al. (2001)
2/3 inhib. int. → 2/3 inhib. int.	Normalize 2/3 inhibition (2-against-1 principle)	Tamas et al. (1998) ; Fukuda et al. (2006)

The present article models how perceptual grouping of boundaries emerges in a laminar cortical model of spiking neurons. Spiking neurons challenge the bipole property because communication using temporally discrete, not necessarily coincident, spikes from multiple cells increases the difficulty of computing whether two or more inducers are contributing to the formation of grouping. Indeed, multiple cells with different axonal delays contribute to boundary completion on either side of a target cell, yet a target bipole cell must somehow distinguish whether spikes converge on it from opposite sides of its cell body (which may cause boundary completion) or from a single side (which does not cause boundary completion). Just the fact of spike coincidence cannot explain this distinction.

Reconciling Fast Feedforward and Slower Feedback Processing. Some recent models and experimental studies challenge the idea that visual contours emerge through gradual accumulation of feedforward and feedback signals over time. Some models postulate that contours are represented by neurons that emit coincident spikes, rather than by the strength of their firing rates (Yen et al. 1999). Others hypothesize that the first feedforward wave of activity following stimulus onset is sufficient to represent boundary contours (VanRullen et al., 2001). Consistent with this perspective, face-selective neurons in primate inferotemporal cortex show significant selectivity for a target face 80-100ms after stimulus onset (Oram and Perrett 1992). Such results are claimed to support a view of the brain in which perception is the result of a single feedforward wave of activity where retinal input to LGN, V1, V2 and V4, and to IT takes

no more than 10ms between successive synaptic stages. Due to this stringent limit on processing time, it has been suggested that the order at which neurons in a population emit their first spike after stimulus onset, rather than their firing rate, codes for various dimensions of that stimulus (Thorpe et al. 2001; VanRullen et al. 2005).

On the other hand, such a view is not compatible with a large number of perceptual experiments. For example, psychophysical experiments that have tried to estimate the amount of time required for illusory contour completion have yielded much slower processing times. One paradigm is that of primed-matching, in which a contour prime is presented prior to a test pair, and where the subject's task is to indicate whether the stimuli in the test pair are the same or not. Contour completion time is assessed by measuring how long an illusory contour prime must be presented for its priming effect to reach the same level as that of a corresponding real contour prime. In an initial study employing this paradigm, completion times of 75-200ms were found (Sekuler and Palmer 1992). A later study highlighted the dependence of completion time on the size of the illusory contour gap, such that completion took somewhere between 255 and 450ms for the largest gap studied in that experiment (Guttman et al. 2001). Another method compared the decay of persistence between real and illusory contours. Whereas for real contours persistence duration diminishes monotonically as a function of stimulus presentation, for illusory contours, persistence increases up to a certain presentation time, after which persistence duration diminishes in a manner similar to real contours. The time at which the decay of an illusory contour starts to follow the same course as that of the real contour may be interpreted as the time required for contour completion. Based on this interpretation, Meyer and Ming (1988) found completion times nearing 250ms. Shape discrimination tasks have also been used in which stimuli were chosen so as to require boundary completion for proper discrimination. Such tasks have yielded estimates in the 46-170ms range, depending on stimulus conditions and task particularities (Murray et al. 2001; Ringach and Shapley 1996). Taken together, estimates from these studies suggest that boundary formation is much slower than what would be predicted by the single feedforward spike hypothesis.

Contour bridging cells in V2 take approximately 80ms to respond to illusory contour inducers (Peterhans and von der Heydt 1989), which suggests that their responses emerge from a relatively slow process of temporal integration. Furthermore, these data show that initial spikes are followed by longer lasting and irregular spike trains, possibly indicating the gradual build-up of a robust neural representation, and rendering unlikely the suggestion that strict temporal order codes for contours. In support of this view, awake macaque V1 recordings during presentation of figure-ground stimuli show that, although cortical cells respond to the mere presence of visual features around 57.5ms, their activity is affected by the presence of boundaries only much later, at around 95.0ms (Lamme et al. 1999). Transcranial magnetic pulses applied to early visual areas block the perception of briefly presented stimuli even when applied up to 120ms after stimulus onset, by which time the feedforward sweep is already completed (Lamme and Roelfsema 2000). Feedback may also influence contour formation, as suggested by human brain activation studies during processing of illusory contour figures, which have consistently shown the presence of a wave of feedback activation from temporal areas to V1 and V2 (Halgren et al. 2003; Murray et al. 2002; Yoshino et al. 2006). Against what one might expect from the single feedforward sweep model, higher level cortical areas are activated rather early during stimulus processing, thereby allowing feedback to influence early activity. This is illustrated, for example, by microelectrode recordings in anesthetized monkey in V1, V2 and V3, which reveal that they are

affected by inactivation of MT in the first 10ms after onset of response (Hupé et al. 2001). At an even higher level, MEG recordings obtained in an object recognition task show activity related to correct recognition in orbitofrontal cortex (OFC) 50ms before it is found in fusiform areas which is usually considered to be at a lower level on the feedforward pathway. Moreover, synchrony between OFC and occipital areas appears 80ms after onset, whereas it appears at 130ms between OFC and fusiform areas (Bar et al. 2006). This may be taken to suggest that stable feedforward and feedback interactions involving OFC settle in lower visual areas prior to higher level ones.

Varieties of Brain Feedback: Intralaminar, Interlaminar, Intercortical. Several types of cortical feedback need to be distinguished in order to achieve conceptual clarity: Intralaminar feedback due to recurrent interactions within a single layer of cells, interlaminar feedback from cells in more superficial layers to deeper layers of a single cortical area, and intercortical feedback between cortical areas, which is often called top-down processing.

Early neural models proposed how intercortical top-down attentive feedback can enhance ongoing dynamics when it matches feedforward activity, or reset them otherwise, and trigger fast learning during the match phase (Carpenter & Grossberg, 1993; Grossberg 1976a, 1976b). This Adaptive Resonance Theory, or ART, model also mathematically proved how the initial feedforward choice of a learned recognition category may be confirmed and sharpened by top-down attentive feedback, but that unfamiliar information could drive a memory search for a new category through an iterated reset process. In addition, more resets may occur during a difficult "high vigilance" discrimination task than an easier one. Familiar percepts with little uncertainty could thus be recognized quickly, whereas unfamiliar or more challenging percepts may require longer processing times. Involvement of feedback is therefore proportionally related to task difficulty. This sort of effect was reported in recent electrophysiological recordings in macaque V4 during a task wherein an animal had to detect large (easy to detect) or small (hard to detect) orientation changes of a Gabor stimulus, and under different attentional conditions (stimulus attended vs. unattended). Firing rates obtained were higher in the attended condition than in the unattended condition for hard trials, whereas this difference was smaller for easy trials. (Boudreau et al. 2006). A related proposal, based primarily on perceptual learning studies and summarized as the Reverse Hierarchy Theory (RHT), is that late feedback to low level areas is necessary to refine a crude initial guess at feature binding (Hochstein and Ahissar 2002).

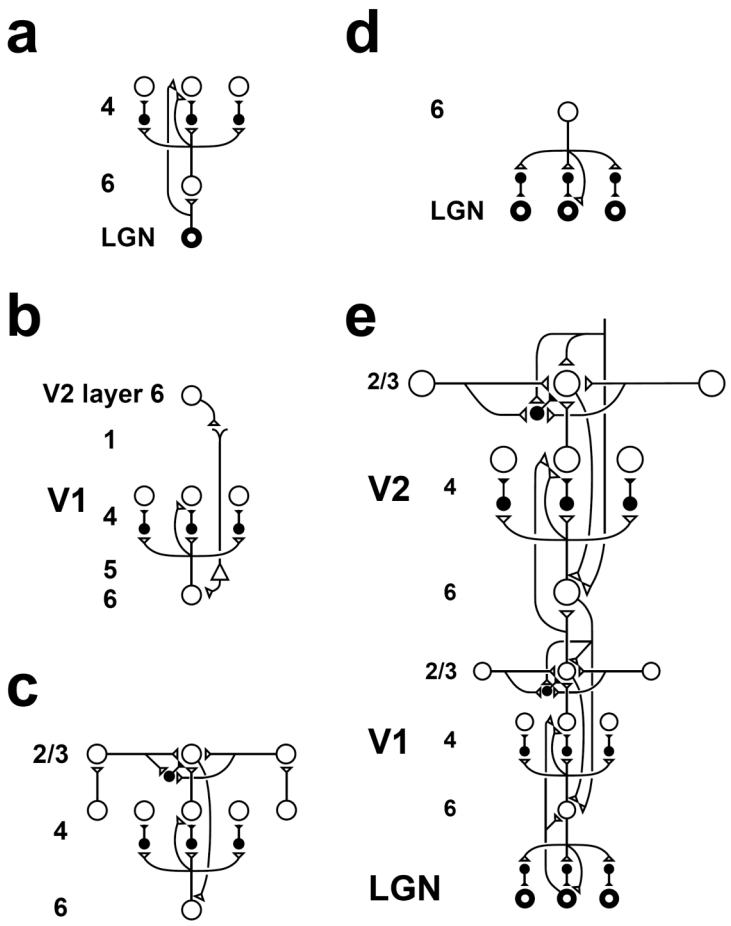

Fig. 2 How known cortical connections join layer 6 → 4 and layer 2/3 building blocks to form an entire V1/V2 LAMINART model. Inhibitory interneurons are shown filled-in black. (a): The LGN provides bottom-up activation to layer 4 via two routes. Firstly, it makes a strong connection directly into layer 4. Secondly, LGN axons send collaterals into layer 6, and thereby also activate layer 4 via the 6 → 4 on-center off-surround path. Thus, the combined effect of the bottom-up LGN pathways is to stimulate layer 4 via an on-center off-surround, which provides divisive contrast normalization (Grossberg 1973, 1980; Heeger 1992) of layer 4 cell responses. (b): Folded feedback carries attentional signals from higher cortex into layer 4 of V1, via the modulatory 6 → 4 path. Corticocortical feedback axons tend preferentially to originate in layer 6 of the higher area and to terminate in the lower cortex's layer 1 (Salin and Bullier 1995, p.110), where they can excite the apical dendrites of layer 5 pyramidal cells whose axons send collaterals into layer 6 (the triangle in the figure represents such a layer 5 pyramidal cell). Several other routes through which feedback can pass into V1 layer 6 exist. Having arrived in layer 6, the feedback is then "folded" back up into the feedforward stream by passing through the 6 → 4 on-center off-surround path (Bullier et al. 1996). (c): Connecting the 6 → 4 on-center off-surround to the layer 2/3 grouping circuit: like-oriented layer 4 simple cells with opposite contrast polarities compete (not shown) before generating half-wave rectified outputs that converge onto layer 2/3 complex cells in the column above them. Like attentional signals from higher cortex, groupings which form within layer 2/3 also send activation into the folded feedback path, to enhance their own positions in layer 4 beneath them via the 6 → 4 on-center,

and to suppress input to other groupings via the 6 → 4 off-surround. There exist direct layer 2/3 → 6 connections in macaque V1, as well as indirect routes via layer 5. (d): Top-down corticogeniculate feedback from V1 layer 6 to LGN also has an on-center off-surround anatomy, similar to the 6 → 4 path. The on-center feedback selectively enhances LGN cells that are consistent with the activation that they cause (Sillito et al. 1994), and the off-surround contributes to length-sensitive (endstopped) responses that facilitate grouping perpendicular to line ends. (e): The entire V1/V2 circuit: V2 repeats the laminar pattern of V1 circuitry, but at a larger spatial scale. In particular, the horizontal layer 2/3 connections have a longer range in V2, allowing above-threshold perceptual groupings between more widely spaced inducing stimuli to form (Amir et al. 1993). V1 layer 2/3 projects up to V2 layers 6 and 4, just as LGN projects to layers 6 an 4 of V1. Higher cortical areas send feedback into V2 which ultimately reaches layer 6, just as V2 feedback acts on layer 6 of V1 (Sandell and Schiller 1982). Feedback paths from higher cortical areas straight into V1 (not shown) can complement and enhance feedback from V2 into V1. [Reprinted with permission from Raizada and Grossberg 2001.]

Laminar cortical models enable a finer analysis of intracortical processing. The circuitry of the LAMINART model (Figure 2; Grossberg, 1999, 2003, 2007; Grossberg, Mingolla & Ross 1997; Grossberg & Raizada 2000; Raizada & Grossberg 2001, 2003; Yazdanbakhsh & Grossberg 2004) shows how a fast feedforward sweep of activation throughout a cortical hierarchy could occur in response to unambiguous information, consistent with the results of Thorpe et al. (2001); see Figure 2e wherein layers 4-to-2/3 in one cortical area project to layers 4-to-2/3 in the next, and so on. However, in response to ambiguous information, self-normalizing competition among alternative cortical interpretations of the data may weaken the activation amplitude and coherence of each alternative, thereby slowing down its processing, and enabling interlaminar, but intracortical, feedback (Figure 2c) to contrast-enhance and thereby choose the alternatives that are supported by the most evidence, thereupon automatically speeding up processing of those choices. These properties clarify an important sense in which the cortex "runs as fast as it can" given the degree of uncertainty in the data. It also shows how the brain goes beyond current Bayesian models to implement a kind of real-time probability theory and hypothesis testing that can deal with ambiguous environments whose rules can change rapidly through time.

In particular, the LAMINART model clarifies how a real boundary in an image may be formed with a fast feedforward sweep of activation from layers 4-to-2/3 and then on to layers 4-to-2/3 in subsequent cortical areas. In contrast, completion of an *unambiguous* illusory contour would require intralaminar feedback within a recurrent network using long-range horizontal connections within layer 2/3 (Figure 2c), and could thus take considerably longer. Completion of an *ambiguous* illusory contour in an image with multiple possible groupings could, in addition to intralaminar feedback within layer 2/3, use interlaminar feedback between layers 2/3, 6, and 4 (Figure 2c) to resolve the ambiguity. Feedback from the deeper 6-to-4 layers includes self-normalizing competitive interactions that, along with the positive feedback within layer 2/3 and between layers 2/3-to-6-to-4, help to choose among possible perceptual groupings. In addition, during both real and illusory contour formation, such a laminar cortical circuit may use intralaminar long-range interactions and interlaminar competitive interactions to synchronize signals that may be temporally dispersed due to different axonal and synaptic delays (Yazdanbakhsh and Grossberg 2004).

However, all of these results about boundary completion and illusory contour formation used rate-based models. What cortical mechanisms allow the bipole property to be realized in a spiking milieu? It is not sufficient to base such an analysis on the possibility that individual spikes may be coincident if only because outputs from multiple cells at multiple distances and time lags input to each bipole grouping cell from each side of its receptive field, and because the time scale of conscious perceptual grouping is orders of magnitude slower than the time scale of individual spiking coincidences.

Our study extends the LAMINART model to explain and quantitatively simulate parametric neurophysiological data about how spike-based cortical grouping may occur. This extended model represents a synthesis of the LAMINART model and the Synchronous Matching ART (SMART) model of Grossberg and Versace (2008). The SMART model has already simulated how spiking dynamics in laminar cortical circuits can explain databases other than those about perceptual grouping. In particular, SMART clarifies how bottom-up adaptive filtering and top-down attentive learned expectation processes undergo match/mismatch operations that attentively regulate perceptual and cognitive processes, notably how multiple stages of laminar cortical processing interact with specific and nonspecific thalamic nuclei to control category learning and recognition, and how gamma and beta oscillations may be triggered in match and mismatch states, respectively. The current study focuses on the horizontal interactions that support perceptual grouping, rather than the bottom-up/top-down processes that regulate attention. A future study will synthesize both types of processes into a more comprehensive cortical model of how spiking dynamics are regulated in bottom-up, horizontal, and top-down laminar interactions.

Previous LAMINART modeling work simulated how cortical layer 2/3 pyramidal cells respond to inputs from deeper cortical layers to group together (almost) collinear image features via long-range recurrent excitatory interactions between the pyramidal cells. This long-range oriented interaction limits contextual contributions to a restricted set of neighboring collinear layer 2/3 cells with a similar orientation preference and (almost) collinear positional alignment, as has been experimentally found (Table 1). Figure 1C illustrates how a pair of collinear pac man figures can activate bipole cells located between them to form an illusory contour. Similar grouping kernels have been reported by several authors (e.g. Field et al. 1993; Li 1998). If only excitatory recurrent connections existed, run-away excitation could easily occur. This is prevented by balancing recurrent interactions between layer 2/3 long-range excitatory pyramidal cells and short-range inhibitory interneurons. Together, these inhibitory and excitatory interactions ensure that single-sided input, however strong, does not lead to horizontal activation (Figure 1B). An excitatory-inhibitory balance also implies that inhibition is not too strong, thereby preventing maladaptive suppression of network activation. Earlier modeling has shown how such an excitatory-inhibitory balance can self-organize during cortical development and give rise to a laminar perceptual grouping circuit whose properties match perceptual data from adult human observers (Grossberg and Williamson 2001). This analysis illustrates how adult perceptual properties may emerge from the dynamics that govern stable brain development.

The distinction between the initial feedforward sweep and subsequent feedback interactions in the processing of contours is illustrated in Figure 3, where interneurons have been omitted for clarity. Bottom-up input to layer 2/3 bipole cells is provided by cells in layer 4 (see also Figure 4). In the case of a real contour (Figure 3A), the first feedforward sweep activates layer 2/3 bipoles at all input-recipient cells, since each bipole cell then receives direct bottom-up input from layer 4. In the case of an illusory contour (Figure 3B), the bipoles that are located

over the illusory contour gap receive indirect input from neighboring bipoles after the latter are activated by the first feedforward sweep. A stable boundary representation then emerges due to subsequent recurrent feedback via horizontal connections within layer 2/3 (Figure 3C). Because an illusory contour receives indirect horizontal input, rather than the more direct input to a real contour, the first spike occurs much later in the middle of an illusory contour than of a real contour (Figure 3D). The results in Figure 3D were obtained by simulating illusory and real contours and computing the difference in first spike latency of a cell located in the middle of the contour. Nonzero input was applied at nine contiguous locations for the real contours, whereas the three locations in the middle were reset to zero for illusory contours. Both types of contours were simulated at current input strengths ranging between 0.0084nA and 0.12nA. The simulations indicate that the latency difference between illusory and real contours remains large (> 50ms) at all input strengths.

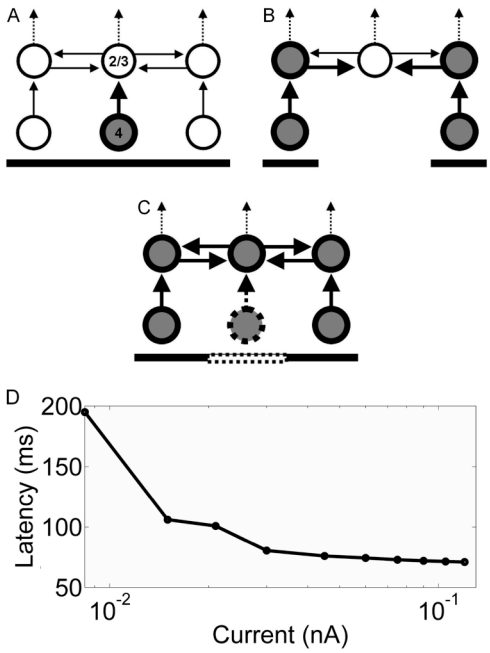

Fig. 3 Feedforward and feedback interactions in the bipole network for real and illusory contours. (A) Upon presentation of a real contour, a single feedforward wave of activity is sufficient to activate a bipole cell located in the middle of the contour via direct input from layer 4 (indicated in gray). (B) In comparison, bipoles located over an illusory contour gap receive only indirect excitation through layer 2/3 horizontal connections during the initial feedforward wave. This results in an increase in latency until the first middle bipole spike, compared to the real contour case. (C) After initial feedforward propagation, horizontal feedback from the middle bipoles in layer 2/3 contributes to strengthen boundary representations whether for real or illusory contours (denoted as dashed lines). (D) Difference between illusory and real contours in the latency of the first spike of the bipole cell located in the middle of the contour. The first spike always occurs later for illusory contours and at all current inputs, due to indirect activation through horizontal connections in the first feedforward wave of activation.

Feedback from higher cortical areas to lower ones enables interaction of grouping circuits at different spatial scales. For example, activation of smaller-scale bipole cells in V1 is modulated by feedback from larger-scale bipole cells in V2, such that contextual elements at a larger spatial

scale may sharpen the activity at the level of V1 bipole cells (Anzai et al. 2007; Grossberg and Raizada 2000; Grossberg and Swaminathan 2004; Kisvárday et al. 1997; Raizada and Grossberg 2001; Shmuel et al. 2005). Although this article models neurophysiological data about V1 horizontal interactions, the similarity of V1 and V2 circuits with respect to the presence of anisotropic horizontal collaterals suggests that variants of our results may also apply to V2. Table 2 lists supporting evidence from various species for the presence of bipole-type kernels in both V1 and V2. The kernels were chosen with the following considerations in mind: the extent of horizontal connections in layer 2/3, the approximate width of a hypercolumn, and the fact that each spatial location in the model represents one hypercolumn. Based on the data reviewed in Table 2, the extent of horizontal connections is estimated to be of approximately 7mm, with a hypercolumn width of 1mm, which is consistent with previous estimates (e.g. Yazdanbakhsh and Grossberg, 2004). Based on these numbers, the horizontal kernels were chosen to span 7 spatial locations. Kernels of this size were also used in Grossberg and Swaminathan (2004).

Table 2 Maximal bilateral extent of horizontal connections from selected studies.

Species	**Area**	**Horizontal extent [mm]**	**Selected references**
Cat	Area 17	8	Gilbert et al. (1983)
	Area 18	6.5[a]	Kisvárday et al. (1997)
Tree shrew	V1	8	Bosking et al. (1997)
Monkey	V1	7	Stetter et al. (2002)
	V2	8	Levitt et al. (1994)

The current Spiking LAMINART model (sLAMINART) uses Hodgkin-Huxley (1952) dynamics to represent realistic neuronal biophysical membrane constraints (cf. Gautrais and Thorpe 1998). The model depends upon intracellular dynamics to temporally average across irregularities in individual spike timing, and to thereby enable bipole grouping to occur in response to approximately coincident bursts of spikes. The prevention of outward spreading of activation in response to individual image inducers also exploits spiking mechanisms. Hodgkin-Huxley type cells can behave as threshold units due to the presence of a stable attractor state during a period with little or no input (Carpenter 1979; FitzHugh 1955; Izhikevich 2007). Thresholds help to minimize noise propagation, which is critical for robustness in networks with multiple layers (Sarpeshkar 1998). Previous rate-based bipole models used an explicit rectification, or threshold,

[a] Although the estimated horizontal extent appears smaller for area 18 than for area 17, the lower cortical magnification factor in area 18 (0.75 $mm^2/degrees^2$ for area 18 Vs 3.6 $mm^2/degrees^2$ for area 17 near area centralis; Tusa et al. 1979) means that horizontal connections in that area span a wider range of visual angle, and thus can be considered as functioning at a larger scale.

to prevent boundary propagation in response to individual inducers. In sLAMINART, such rectification is implicit and derives from Hodgkin-Huxley membrane dynamics within each cell.

Each cell's intracellular dynamics supports a graded, or analog, activation profile. A critical property of a properly designed network is that it retains analog sensitivity even as it binds multiple cell activations together into emergent groupings through recurrent interactions. Such a coexistence of analog sensitivity with coherent binding is called *analog coherence*, and helps to explain effects of contrast magnitude on perceptual grouping (Grossberg et al. 1997; Grossberg 1999). sLAMINART successfully simulates a range of single-cell recording data about analog-sensitive perceptual grouping, and hereby shows how digital spiking dynamics can induce analog coherence. In particular, sLAMINART quantitatively simulates data about short-range grouping (Kapadia et al. 2000), long-range modulation (Crook et al. 2002; Polat et al. 1998), contrast sensitivity (Polat et al. 1998), horizontal summation (Chisum et al. 2003), and gamma-range oscillations (Gray et al. 1989). The next section describes the sLAMINART model, followed by a section that summarizes model simulations.

2 Method

The sLAMINART model defines and simulates a layer 2/3 spiking bipole grouping circuit, fed by inputs from deeper cortical layers, described for simplicity as layer 4 in Figure 4. Each spatial location along the horizontal axis roughly corresponds to one hypercolumn. Pyramidal cells mutually excite each other via long-range horizontal connections. Inhibitory interneurons in each hypercolumn are divided into two populations. As shown in Figure 4, one population receives excitatory long-range horizontal input from layer 2/3 pyramidal cells in hypercolumns located to their left. The other population receives excitatory long-range horizontal inputs from layer 2/3 pyramidal cells located to their right. Henceforth we refer to the two populations of interneurons as *Left* and *Right*, respectively. Each layer 2/3 inhibitory interneuron inhibits the layer 2/3 pyramidal cell and the antagonist interneuron in the same hypercolumn. This inhibitory scheme is designed to realize the bipole property within a laminar cortical circuit (Grossberg and Raizada 2000; Raizada and Grossberg 2001).

For example, when a pyramidal cell receives input from a single excitatory pyramidal cell to its left, it also receives a balanced inhibitory input from its Left inhibitory interneuron ("one against one"). Hence, individual pyramidal cells cannot cause run-away excitation across the network due to the way in which the pyramidal cell temporally averages the excitatory and inhibitory spikes. When a pyramidal cell receives collinear inputs from excitatory pyramidal cells to its left and its right, these flanking pyramidal cells activate the corresponding Left and Right inhibitory interneurons. Both of these interneurons inhibit the target pyramidal cell, as well as one another. The mutual inhibition of the inhibitory interneurons acts to normalize their total activity (Grossberg 1973). As a result, the total excitation to the target pyramidal cell increases, but the total inhibition remains similar to the level of inhibition from an individual inhibitory interneuron ("two against one"). The target pyramidal cell can therefore fire, again due to the way in which the pyramidal cell temporally averages the excitatory and inhibitory spikes.

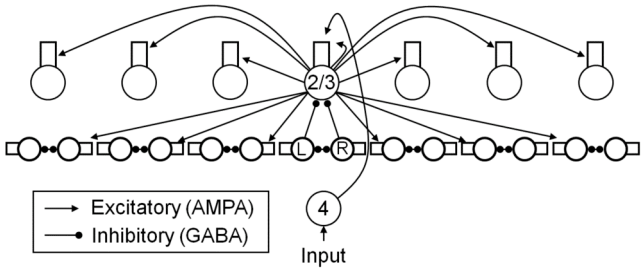

Fig. 4 Bipole cell circuit: Input is clamped at each spatial location at the level of Layer 4 pyramidal cells. Each layer 4 pyramidal cell projects to the dendrite of a single layer 2/3 pyramidal cell. The pyramidal cell dendrite also receives horizontal excitatory connections from neighboring layer 2/3 pyramidal cells, including projections from itself. Layer 2/3 horizontal connections also excite the dendrites of left or right inhibitory interneurons, which inhibit neighboring layer 2/3 pyramidal cell bodies and right or left inhibitory interneuron cell bodies. See Appendix equations (11)-(17).

Each layer of the model is composed of a one-dimensional array of 51 neurons. Layer size is much larger than the largest input stimulus simulated here (13 contiguous spatial locations) in order to prevent boundary effects which could have resulted from horizontal interactions. Layer 4 cells are implemented with a single somatic compartment governed by Hodgkin-Huxley dynamics. External input to the model is provided via current injection in the soma of layer 4 cells. Pyramidal cells and interneurons in layer 2/3 have an additional passive dendritic compartment, which is consistent with pyramidal cell anatomy and enables smoother temporal integration of excitatory inputs from other pyramidal cells. This smoother integration results from the cable equation, whose leaky integrator dynamics ensure that both the temporal integration of inputs from pre-synaptic afferents into the dendritic compartment, and the transfer of current from the dendrite to the soma, are much slower than individual spike events.

Smooth integration is needed to obtain stable grouping in the presence of pre-synaptic spikes that are not coincident due to distance-dependent axonal delays and the presence of noise. Besides providing better stability, the presence of a dendritic compartment also allows selective enhancement of inhibition by inhibitory synapses on the soma, while excitatory synapses terminate on the dendrite (Megías et al. 2001; Spruston 2008). This anatomy allows inhibition to reach the soma faster than excitation, thereby helping to prevent spurious outward propagation of activity. Another consequence of this specific placement of synapses is to make the spike trains of bipole cells look like that of bursting cells, although they are not intrinsic bursters. Indeed, the occurrence of an inhibitory spike to the soma of an excited bipole cell is strong enough to induce a pause in that cell's otherwise constant firing activity, yielding spike trains similar in appearance to various types of intrinsic bursters (Carpenter 1979).

Synaptic interactions are implemented as double exponentials with parameters corresponding to α-amino-3-hydroxy-5-methylisoxazolepropionic acid (AMPA) and γ-amino-butyric Acid (GABA) receptors for excitatory and inhibitory synapses, respectively. The location of synaptic contacts is on the passive dendrite for AMPAergic synapses and on the soma for GABAergic synapses. The model includes realistic distance-dependent axonal delays (Bringuier et al. 1999; Girard et al. 2001; Hirsch et al. 1991). Mathematical equations and parameters, as well as details pertaining to the simulation protocol, are included in the Appendix. All

simulations were conducted using *KDE Integrated Neurosimulation software* (KInNeSS; Versace et al. 2008).

3 Results

3.1 Illusory contour

The combination of the above factors, notably the bipole-organized balance of excitation and inhibition, intracellular temporal spike averaging, and the differential locations of excitatory and inhibitory contacts on soma and dendrite, respectively, supports stable firing of layer 2/3 spiking bipole cells during grouping of an illusory contour (Figure 5). The bottom plot of Figure 5 shows a 1D stimulus pattern corresponding to two collinear flanking stimuli (each 3 spatial locations wide) separated by a wide gap (5 spatial locations). Inducers were simulated by injecting 0.03nA current inputs into layer 4 pyramidal cells. The middle plot shows the firing rate of layer 4 pyramidal cells, where completion does not occur. Note, unless noted otherwise, reported firing rates are computed over 500ms of simulation following an initial transient. The upper plot shows the firing rate of layer 2/3 bipole cells, where inward completion is present. Adding small amounts of noise in layer 2/3 dendrites leads to negligible activity in a few cells located just outside of the stimulus pattern.

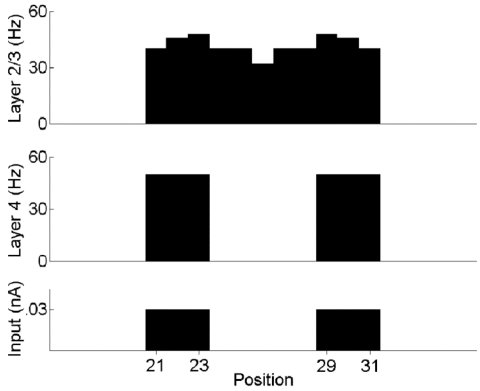

Fig. 5 Long-range completion in layer 2/3 spiking bipole cells: Two flanking stimuli (bottom) separated by a wide gap (5 hypercolumns) give rise to corresponding activity in layer 4 pyramidal cells (middle). The layer cell activities generate inputs activity pattern to vertically aligned layer 2/3 bipole cells (top), whose activation leads to inward completion of activity. Note the absence of outward propagation of activity. See text for further details.

3.2 Short-range grouping

Spatially short-range grouping is illustrated in Figure 6, where model simulations are plotted together with monkey V1 data from three different conditions: *flankers-only*, *target-only*, and *target-with-flankers* (Kapadia et al. 2000). The size of the illusory contour gap and of the inducers in these simulations was determined by taking into consideration the cortical magnification factor and details about the original experimental protocol. In particular, the gap and inducers both cover one spatial location in the simulations; see the Appendix. In the flankers-only condition, two bars were presented adjacent to the *classical receptive field* (CRF) of a recorded cell.

Note that the firing rate in the flankers-only grouping simulation of Figure 5 is higher than that shown in Figure 6. This is due to several interacting factors: First, the simulated illusory contour gap is wider in Figure 5 than in Figure 6, but the inducer length is also wider. Second, the horizontal projections are weaker than the bottom-up projections (in Table 3, g_{max} equals 0.003 and 0.049 for horizontal and bottom-up projections, respectively)**.** Thus, although the amount of current input in Figure 5 was the same as in the high contrast conditions of Figure 6 (0.03nA in both cases, denoted as 50% contrast in Figure 6), the amount of support is greater in Figure 5, resulting in a higher firing rate in that case due to horizontal summation of wider bottom-up inputs.

Table 3 Synaptic connections parameters. Weights (W) and delays delays (δ_{Ax}) of horizontal connections are determined by equations (19) and (20) respectively.

Pre-Synaptic	**Post-Synaptic**	**Post-synaptic Site**	**E [mV]**	**g_{max} [mS/cm^2]**	**τ_r [ms]**	**τ_f [ms]**	**w**	**δ_{Ax} [ms]**
4 pyr.	2/3 pyr.	dendrite	0	0.049	2	4	0.2	3
2/3 pyr.	2/3 pyr.	dendrite	0	0.003	2	6.5	--	--
2/3 pyr.	2/3 int.	dendrite	0	0.037	1	4	--	--
2/3 int.	2/3 pyr.	soma	-60	1.8	2	7	1	1
2/3 int.	2/3 int.	soma	-70	1	2	7	1	0.1

The model explains the three cases depicted in Figure 6 as follows. In the flankers-only condition, summation of horizontal inputs leads only to weak increments in firing rates, compared to the other two conditions, as noted above. Just as excitatory horizontal input is weak, inhibitory input to the target bipole is also weak, since interneurons in the target hypercolumn inhibit each other through recurrent connections. This balance of excitation and inhibition enables the target bipole to emit spike trains, resulting in short-range grouping. In the target-only condition, bottom-up input from the layer 4 cell activates the layer 2/3 bipole across a wide dynamic range. The reason why the range of firing rate is greater in this condition than in the other two is that it is the only one where inhibitory interneurons in the hypercolumn of the recorded bipole cell do not receive excitatory inputs from neighboring hypercolumns. Given the graded activity profile of single Hodgkin-Huxley cells modeled here (see Figure 13 in the Appendix), the target bipole cell is thus free to span a wide range of firing rates. Finally, in the target-with-flankers condition, strong bottom-up input coupled with horizontal interactions results in a somewhat reduced dynamic range. The bottom-up and flanker inputs activate horizontal excitatory connections to all bipole cells in between. These recurrent excitatory horizontal interactions cause a larger activation of the target cell even at low contrast. In addition, inhibitory interneurons in the target hypercolumn receive bilateral horizontal inputs. As a result, the interneurons inhibit each other through recurrent connections, as in the flankers-only condition. As contrast increases, the activity of the excitatory recurrent interactions and the inhibitory interneurons increases until the inhibitory interneuron activities reach the self-normalizing range, thereby helping to limit the increasing firing rate of the target bipole.

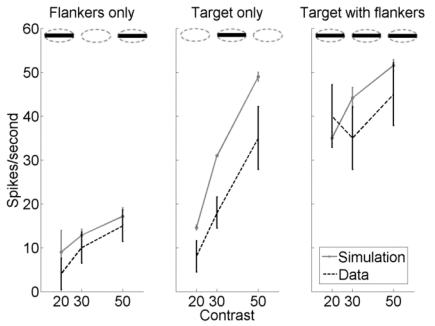

Fig. 6 Data from Kapadia et al. (2000) (dashed lines, reprinted with permission) and model simulations (solid lines). Error bars for the data represent variations among different cells/trials. Error bars for simulations represent variations among different parameter settings (see Appendix). The stimulus pattern in each case is indicated in the insets. See text for further details

3.3 Long-range modulation: Two sides

At greater stimulus separations, contrast-dependent long-range modulation has been reported in pyramidal cells of area 17 (V1) in the cat (Polat et al. 1998). In that study, the activity of a target cell whose receptive field was stimulated with an optimally oriented bar was monitored in the absence or presence of flanking collinear stimuli. The stimulus bars were made long enough to cover the entire classical receptive field (CRF) of the recorded cell. In simulations, the bars span 3 spatial locations. At low stimulus contrast, flanking inputs increased the activity of the target cell located between them, relative to when flankers are absent (facilitation condition), whereas at high stimulus contrast, they resulted in depression of activity relative to the no-flanker case. In the experiment, the separation between the flankers was determined by successively widening the gap until no grouping was observed. In the simulations, this occurred when the gap was widened to the point that it spanned 7 spatial locations, whereas grouping with gaps of width 5 and 1 have been obtained in Figures 5 and 6, respectively. Figure 7 shows that the model simulates these data.

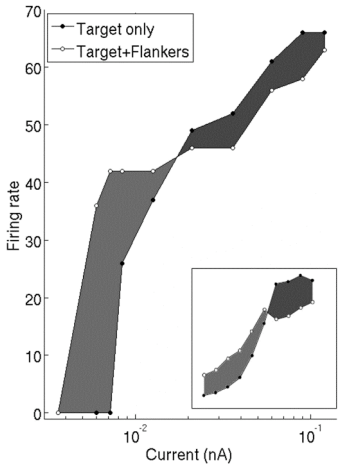

Fig. 7 Horizontal projections limit analog sensitivity over long distances. This is indicated by a flatter slope over most contrasts tested in the target-plus-flankers condition than in the target-only condition. The simulated activity can be compared to a sample result from Polat et al. (1998) shown in the inset. [Data reprinted with permission from Polat et al. (1998).]

This result may be explained as follows: As in the target vs. target-with-flankers conditions of Figure 6, target bipole firing is higher at low current input in the target-with-flankers. As current input to the target site increases, the inhibition on the target cell body from flanking interneurons limits the combined influence of bottom-up and horizontal excitatory inputs from further increasing target bipole activity. Figure 7 shows that, as current input increases, this limiting influence eventually results in greater target bipole activity in the target-only condition than in the target-with-flankers condition. Such reversal of activity is not observed in the simulations of Figure 6, where current input is not sufficiently high (the maximum current input is 0.03nA in Figure 6 whereas it is 0.12nA in Figure 7).

3.4 Long-range modulation: One side

The bipole property can also enable one pyramidal cell to modulate the activity of a horizontally displaced cell, even though an individual pyramidal cell cannot cause significant suprathreshold grouping activity. Figure 8 reports simulation results and supporting evidence for this property from a cat V1 pyramidal cell (data from Crook et al. 2002). Unlike the previous experiments which employed pairs of flankers, the data and simulations in Figure 8 use a single flanker. In the *target-only* condition, a single optimally oriented bar was presented in the CRF of the target cell. In simulations, this bar length spans a single spatial location. In the *flanker-only* condition, a single collinearly oriented bar was presented in a location adjacent to the CRF of the cell. In the *target-with-flanker* condition, the target and flanker bars were presented simultaneously. The contrast of the flanker bar was 10 times higher than the contrast of the target bar. In simulations, current input to the target and flankers was 0.0096nA and 0.06nA, respectively, in order to approach this ratio. Finally, in the *GABA* condition, both the flanker and target bars were presented but with a simultaneous injection of GABA at the cortical activation site of the flanker stimulus.

As expected, cell activity was high in the *target-only* condition. In the model, this was due to bottom-up activation of the target layer 2/3 pyramidal cell. Activity of the target pyramidal cell was decreased to near zero in the *flanker-only* condition, reflecting the absence of outward completion from the flanker. In simulations, activity decreased to zero since, although flanker input to the target hypercolumn simultaneously excited the bipole cell and one inhibitory interneuron, the synaptic weights on the path leading to inhibition of the target bipole are stronger. Indeed, the maximal conductance g_{max} of layer 2/3 horizontal projections between model pyramidal cells is 0.003μS, whereas the maximal conductances for the pyramidal-to-interneuron and interneuron-to-pyramidal projections are 0.037μS and 1.8μS, respectively (see Table 3). In comparison, in the flankers-only condition of Figure 6, *bilateral* excitatory input caused the interneurons to inhibit each other due to the recurrent connectivity, thereby leaving the bipole cell free to spike at a low level in that case.

Firing rates in Figure 8 nearly doubled in the *target-with-flanker* condition, relative to the target-only condition. As in Figure 6, there is super-additive excitation in the target-with-flankers case. In Figure 8, this is due to recurrent horizontal excitatory connections between the single flanker and the target cell, after bottom-up excitatory input from layer 4 to the target bipole cell allows it to overcome inhibition from the flanker site and to emit spikes. If GABA inhibits the flankers, then the target cell response returns to the level in the target-only condition.

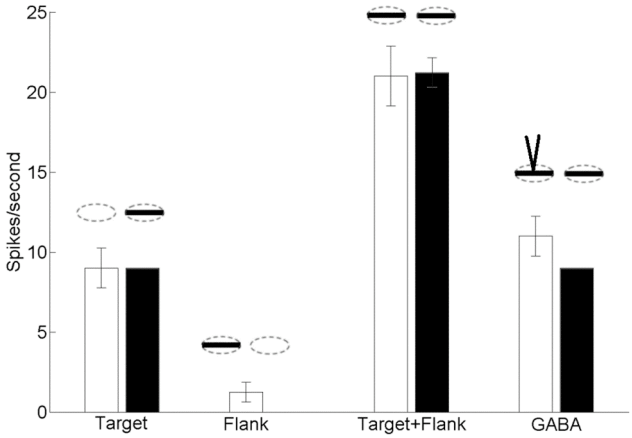

Fig. 8 Crook et al. (2002) neurophysiological data (empty bars) is matched with simulations (dark bars) in four conditions. Note the absence of outward propagation in the flanker-only condition. Error bars for the data represent the variation observed across different cells/trials, whereas they represent variations across different parameter settings for the simulations (see Appendix). [Data reprinted with permission from Crook et al. (2002).]

3.5 Horizontal summation

The salience and strength of perceptual groupings depend upon the amount of *support* present in the image inducers (Lesher and Mingolla 1993; Soriano et al. 1996). Support is the ratio of the length of inducers to the total stimulus length. A correlate of this psychological observation is shown in physiological recordings of a layer 2/3 pyramidal cell in the tree shrew (Chisum et al. 2003). In this experiment, cell activity was monitored during presentation of stimulus bars of different lengths and at a predefined contrast level. Activation was reported as the ratio of firing activity obtained for the various stimulus lengths divided by the activity obtained for a wider bar of higher contrast. Figure 9 shows model bipole cell activity as a function of the length (in degrees of visual angle) of the stimulus presented at different contrast levels (the contrast levels tested correspond to current inputs of 0.0084, 0.0126 and 0.03nA) and overlaid on a subset of the Chisum et al. (2003) data. Horizontal summation is indicated by the fact that, as the array width gradually increases from one spatial location to seven, relative activity with respect to a long high contrast stimulus bar (13 spatial locations wide, current input of 0.048nA), tends toward 1. See the Appendix for details on how the degrees of visual angle from the experimental study were matched to the number of locations spanned in present simulations.

This result may be explained by noting that the target bipole cell receives excitatory input from a progressively larger number of flanking bipole cells as the stimulus bar gets wider. At low contrast, excitation from horizontal projections is slightly stronger than inhibition, which results in an increase in target bipole firing rate as a function of inducer length. However, at the highest level of contrast tested, the influence of inhibition becomes more pronounced, such that further increasing the inducer length does not increase the activity of the target bipole. Note in particular how the relative activity plotted for this contrast level approximates 1, meaning that it approaches the activity obtained in the case of the 13-units wide bar at even higher contrast. The model thus predicts that horizontal summation exerts a significant effect at lower contrasts but

less so at high contrast. This is compatible with the simulations of short-range grouping of Figure 6 and long-range modulation of Figure 7, where the impact of inhibition on the target bipole cell is accentuated at similarly high contrast levels (i.e., for current inputs of 0.03nA), resulting in a reduction in analog sensitivity.

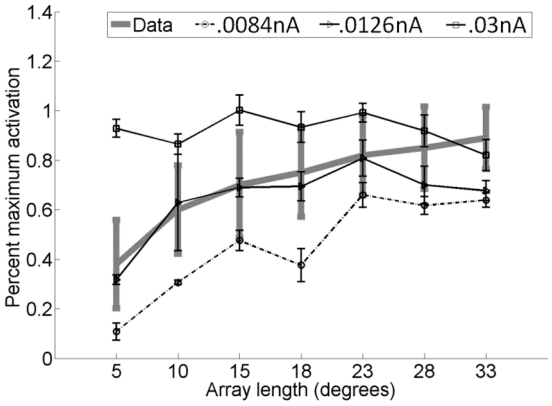

Fig. 9 Activity of a layer 2/3 cell in area V1 of a tree shrew (continuous thick curve) is shown here as the ratio of activity (firing rate) obtained at a particular inducer length with respect to the activity in response to a longer stimulus at high contrast. In the simulations, this baseline stimulus spans 13 hypercolumns and corresponds to a current input of 0.0408 nA. Horizontal summation in the data is consistent with model simulations at lower current inputs (0.0084 and 0.0126 nA), whereas saturation is observed at the high current input simulated (0.03 nA). Error bars in the data represent variations across different cells/trials. They represent variation across different parameters (see Appendix) in the simulations. [Data reprinted with permission from Chisum et al. (2003).]

3.6 Gamma band oscillations, synchrony and perceptual grouping

A number of investigators have reported synchronous oscillations during perceptual grouping, among other brain processes; e.g., Eckhorn et al. (1988) and Gray et al. (1989). Bipole grouping in rate-based models is capable of fast synchronization of boundary groupings, including illusory contours and fast resynchronization after inputs change. Synchronization occurs both in non-laminar models (Grossberg and Grunewald 1997; Grossberg and Somers 1991) and laminar cortical models (Yazdanbakhsh and Grossberg 2004).

To study whether and how resynchronization occurs in the spiking laminar cortical sLAMINART model, simulations were conducted by presenting a random pattern of activation for the first 100ms, thereby randomizing the firing phases of layer 2/3 pyramidal cells, and then switching to either a real contour (Figure 10A) or an illusory contour (Figure 10B). The resulting layer 2/3 membrane potential traces were then low-pass filtered to preserve only burst oscillations. This is consistent with the observation that the oscillations found in the study of Gray et al. (1989) were mostly due to bursts, rather than to single-spike coincidence. Figure 10A shows resynchronization occurring in the 100ms following input change. Figure 10B shows resynchronization to occur around 300ms later. The faster synchronization observed for real contours is due to the fact that layer 4 activity, which drives the activity of layer 2/3, is synchronous along the simulated contour. This result is consistent with data showing that illusory

contours take longer to be perceived than real contours (Francis et al. 1994; Meyer and Ming 1988).

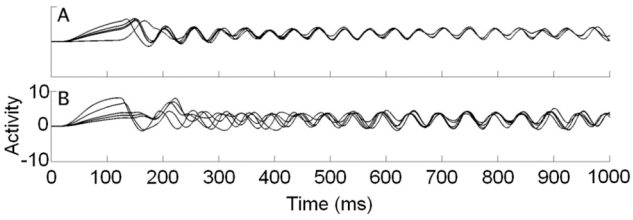

Fig. 10 (A) Fast resynchronization of bursts in the presence of a real contour. A random pattern was presented for the first 100ms and followed by a static real boundary contour stimulus. Oscillations shown here correspond to the middle 5 units along the contour, which was 9 units wide. (B) Slower resynchronization of bursts in the presence of an illusory contour. The gap between inducers was 3 units.

During synchronization, the bipole grouping network exhibits oscillatory synchrony in the low gamma range (>20Hz) along a grouped contour (Figure 11), a claim supported by a wide range of electrophysiological evidence (e.g. Gray et al. 1989; Samonds et al. 2006). This result is related to, but differs in an important way, from the *binding-by-synchrony* hypothesis (Milner 1974; von der Malsburg 1981). In the sLAMINART model, it is more proper to describe a *synchrony-by-binding* hypothesis, since synchronization, when it occurs at all in a bipole network, is an emergent property of how recurrent network interactions bind cells together during perceptual grouping. According to the experimental study of Gray et al. (1989), phase locking between a pair of pyramidal neurons is strongest in area 17 of the cat when a single contour spans the collinear CRF of the two recorded cells (Figure 11, upper left row). Synchrony is reduced at locations on an illusory contour (middle left row), and is non-existent during presentation of uncorrelated moving bars (bottom left row). Simulations (middle column) agree qualitatively with the empirical cross-correlograms.

The single contour condition was simulated as a single inducer, 11 spatial locations wide. For the illusory contour condition, inducer bar and gap length were set to 3 and 5 spatial locations, respectively, as in Figure 5. The uncorrelated bars were simulated by alternately presenting each inducer from the illusory contour condition. Inducers were simulated by injecting 0.03nA current input. A phase randomizing signal was further included by injecting time-varying noise of amplitude up to 0.003nA in the dendrite of layer 2/3 pyramidal cells.

The exact nature of synchronous oscillations in the simulated spike trains is further probed in the right column, where points above the horizontal dashed line indicate significant coherence at a particular frequency (cf. Rosenberg et al. 1989). This analysis confirms the presence of low-range gamma oscillations (20-40Hz) along boundary groupings. Comparison of the single contour and illusory contour conditions reveals that phase-locked layer 4 activity transmitted via layer 2/3 bipole cells located within a pair of nearby layer 2/3 bipoles helps to synchronize activity along the represented contour. This is to be expected from the symmetry of the bipole kernel: bipoles located in the middle project equally strongly to bipoles on the left and right of the contour (see Golubitsky and Stewart (2006) for a discussion of synchrony-inducing symmetry). The spectral analysis in the right column further shows that the shape of the frequency spectrum remains roughly similar across the two conditions. The main difference

resides in the magnitude of the spectrum in each frequency bin, which again reflects the influence of excitation and inhibition from bipole cells in the middle. In other words, both real and illusory contours produce oscillations mainly in the gamma range, but illusory contours display less power overall. However, oscillatory synchrony in this condition remains stronger than in the alternating contour condition, where horizontal excitatory signals from one side of the contour are insufficient to trigger reliable spiking in bipoles on the other side in the absence of concurrent bottom-up input.

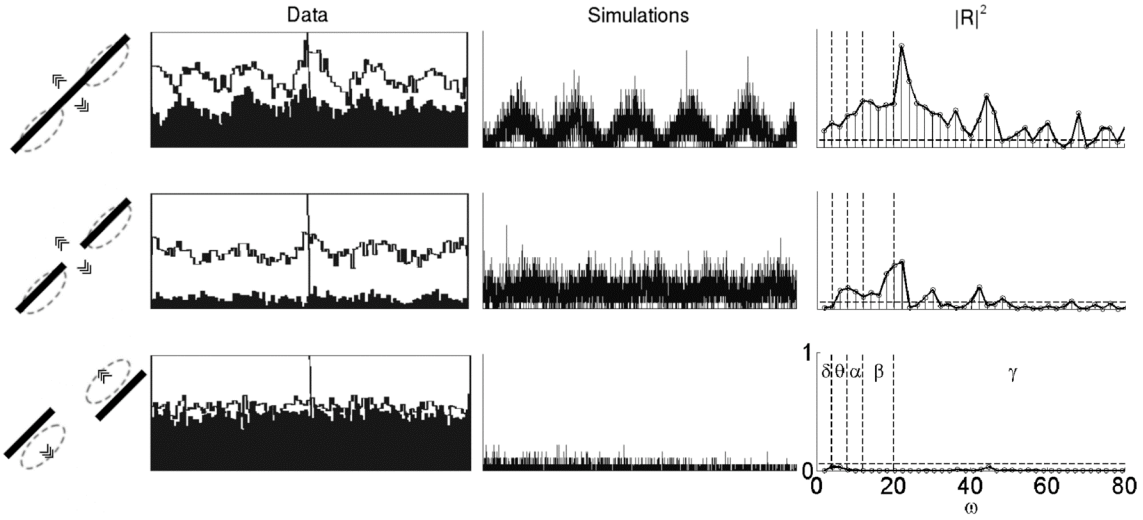

Fig. 11 (Left) Data of Gray et al. (1989) showing that synchrony between pyramidal cells in cat area 17 is strongest for a continuous bar simulus, weaker at an illusory contour induced by a part of collinear bars, and absent between non-collinear bars. (Middle) Model simulations replicate these data. (Right) The synchronous coupling in the model is statistically significant at a confidence level of 5% in the full bar and coherent bar cases and absent in the incoherent bar case, as indicated by the coherence index $|R|^2$. [Data reprinted with permission from Gray et al. (1989)]

The gamma oscillations depicted in Figure 11 remain when measured at a larger scale. In the experimental literature, gamma synchronization of evoked potentials has been found during viewing of grouping stimuli. In particular, Tallon et al. (1995) reported a 30Hz component over areas covering visual cortices in response to a Kanizsa triangle stimulus. In order to probe the synchronous dynamics of the network measured at a larger scale, cell activity across the 1D array of layer 2/3 cells obtained during simulations of an illusory contour (8 units wide flankers separated by a 5 units wide gap) was combined into a single estimate of the local field potential (LFP) according to the methodology described in Versace et al. (2008). The resulting signal was Fourier transformed (FFT) to obtain the power spectrum displayed in Figure 12. This result suggests that the large-scale gamma oscillations observed in response to grouping stimuli may either originate in the bipole circuit, or at least be partially supported by it.

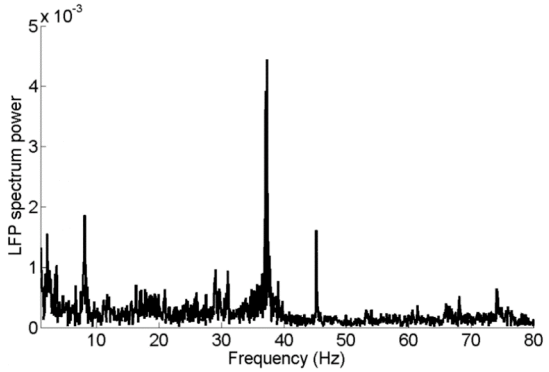

Fig. 12 Local field potential (LFP) spectrum power in model layer 2/3. A clear peak is observed in the low gamma range. This result reflects the pattern of LFP spectrum power obtained using various stimulus configurations. See text for details.

4 Discussion

4.1 Summary of findings

This article demonstrates for the first time how a network of layer 2/3 recurrently interacting spiking neurons with multiple compartments that obey Hodgkin-Huxley dynamics may perform stable, analog coherent, and synchronous perceptual grouping of both real and illusory contours in a manner that quantitatively reproduces key neurophysiological data from multiple laboratories. This sLAMINART model shows how recurrent intralaminar feedback within layer 2/3 responds to initial feedforward activation upon presentation of a grouping stimulus in order to complete a stable boundary representation. Whereas spiking dynamics have in various other models been implemented using highly simplified mechanisms (e.g., integrate-and-fire dynamics in a single dimensionless compartment), the sLAMINART model is defined by more realistic brain mechanisms, including Hodgkin-Huxley cell dynamics, multiple cellular compartments, excitatory and inhibitory recurrent interactions that terminate on cell dendrites and somata, respectively, and distance-dependent axonal delays. In addition, the selective grouping properties that exemplify the bipole property are realized without the use of explicit thresholds, since the latter are implicitly included in Hodgkin-Huxley dynamics for the combination of parameters used here.

The emergence of stable grouping despite the presence of distant-dependent axonal delays and the addition of noise in our simulations demonstrates that perfect coincidence in spike timing is not necessary for grouping to occur. Rather, an instantaneous spike event exerts a temporally persistent influence on bipole cells principally due to the time course of EPSPs and IPSPs (see Appendix equation (10)), and of inter-compartmental currents. These slower processes allow for temporal summation of multiple presynaptic spike trains, thereby enabling the network dynamics as a whole to exhibit properties like analog coherence and sensitivity to the extent of stimulus support.

The differential localization of excitatory and inhibitory terminals on bipole cells, with excitatory synapses on the dendrites and inhibitory synapses on the soma, means that inhibition can act much faster on the soma than excitation does, thereby preventing the unwanted outward

propagation of signals outside of the inducers' locations. This is further guaranteed by the larger conductance of inhibitory synapses than excitatory synapses in the model.

The balance of inhibition and excitation is critical to explain the data on long-range modulation (Figure 7). These data were also simulated in a previous non-spiking laminar cortical model of perceptual grouping by Grossberg and Raizada (2000). That simulation required modulatory feedback from V2 bipole cells to the V1 network. The current study shows how a properly balanced network of spiking layer 2/3 cells within V1 is sufficient to generate this result.

The simulations of fast synchronization highlight the relationship between boundary grouping and gamma oscillations that has been reported in the neurophysiological literature (e.g. Gray et al. 1989; Gray and Singer 1989; Samonds et al. 2006). Gamma oscillations have also been shown to occur in model simulations when a sufficiently good match occurs between bottom-up feature patterns and top-down attentive learned expectations during attentive category learning and recognition (Grossberg and Versace 2008), thereby providing a mechanistic explanation of how gamma oscillations can occur during attentive states (Fries et al. 2001; Gregoriou et al. 2009). These two examples show that gamma synchronization can be the result of quite different brain mechanisms.

These results also argue against a binding-by-synchrony hypothesis. Rather, they illustrate how gamma synchronization may result as an emergent property of functionally distinct types of "binding". Moreover, synchronization need not occur only in the gamma frequency range, even in the same brain network. It may occur in different frequency ranges within the same network due to task constraints. Grossberg and Versace (2008) have predicted, for example, that slower beta oscillations can occur when a mismatch occurs between bottom-up and top-down signal patterns, and at least three laboratories have reported data that are consistent with this prediction (Berke et al. 2008; Buffalo et al. 2004; Buschman and Miller 2008). Grossberg and Versace (2008) have also predicted why more beta oscillations may be found in the deeper layers of visual cortex, as reported by Buffalo et al. (2004), and Grossberg (2009) has proposed an explanation of why beta oscillations occur in the hippocampal place cell learning data of Berke et al. (2008).

4.2 Comparison with other spiking models of grouping

The fact that exact coincidence of spikes is not required in order to represent boundary contours in the model (cf. Figure 10) illustrates that the grouping mechanism is robust. A related mechanism of asynchronous spike-based contour completion – employing long-range anisotropic excitatory connections, but lacking inhibitory interneurons – was proposed in VanRullen et al. (2001). Runaway excitation in the model was prevented by artificially limiting each neuron to emit no more than one spike. Simulations showed that their network can account for cooperation among neighboring collinear inducers (i.e., it can perform contour integration). However, the authors did not test necessary computational properties such as the bipole property, stability of the emergent grouping over time, analog sensitivity, and horizontal summation. In particular, contour persistence is not addressed due to the constraint of a single spike per neuron. Illusory contours are assumed completed as soon as neurons on top of the gap spike once. Since this occurs as a result of fast feedforward accumulation of single spikes from collinear neighbors that receive bottom-up input, it is not clear how much asynchrony the network can tolerate. Another

consequence of the emphasis on fast feedforward integration is that the model predicts that real and illusory contours take approximately the same amount of time to be perceived, which is inconsistent with psychophysical data.

Yen et al. (1999) simulated a more elaborate network of compartmental neurons in which a kernel of long-range anisotropic excitatory connections was used to promote synchronous spiking among populations coding for collinear edges, with the intent of showing how spike timing could be used as an index of which edge a given neuron represents. However, the stimuli used in that study consisted only of real boundary contours. It is not clear whether the network could perform boundary completion, notably illusory contour completion. In addition, the authors did not test for the presence of spurious outward propagation and did not address the requirement of analog coherence.

Yen and Finkel (1998) proposed a model of contour grouping based on synchronization of neural oscillators. However, suprathreshold activation of a cell required direct bottom-up input, implying that their model could not do boundary completion, notably formation of illusory contours. Moreover, in our model, gamma oscillations are an emergent property of cells which, left alone, do not oscillate.

Domijan et al. (2007) implemented a one-dimensional network of non-spiking compartmental bipole cells based on the original Boundary Contour System model of Grossberg and Mingolla (1985a). The dendritic tree of bipole cells in the model was restricted to two branches: one that collects horizontal inputs from the left and the other one from the right. Their simulations replicated the bipole property, analog sensitivity, and horizontal summation. The crucial mechanism consisted in the explicit multiplication of the contribution of both dendritic branches (an AND-gate that preserves analog sensitivity). The model therefore embodies the following two assumptions: (1) the presence of multiplicative interactions between separate dendritic branches, and (2) the anisotropic distribution of postsynaptic sites on the dendrite tree, as dictated by the location of the presynaptic cell (i.e., pre-synaptic inputs from the left target the dendrite on the left, and vice-versa). The first assumption is contradicted by recent experimental findings that supralinear summation occurs only between synaptic sites on a single branch, whereas inputs from different branches sum only linearly (Polsky et al. 2004). The second assumption would be supported if the shape of dendritic trees were anisotropic. However, anatomical evidence suggests that dendritic trees, at least in layer 3 of visual cortices, are isotropic (Elston et al. 1996). Thus it remains to be shown how such an anisotropic distribution of synaptic inputs on isotropic dendritic trees could result from experience-induced development. This model does not incorporate spiking dynamics nor conduction delays, and does not strictly implement the cable equation (e.g., there are no bidirectional interactions between compartments and temporal integration is not present in the dendrites). In other words, the model does not address the problem of how neurons integrate asynchronous spikes to achieve perceptual grouping. Thus, this model does not incorporate several neurophysiological constraints that support sLAMINART quantitative simulations of key neurophysiological data.

5 Conclusion

The sLAMINART model shows how networks of spiking cortical cells in layer 2/3 group collinear contour fragments into unified boundary contours. In particular, simulations show that

the model is able to realize the bipole property, and in doing so, achieves good qualitative and sometimes quantitative agreement with a range of previously published single-cell data about grouping. Perceptual grouping in sLAMINART is temporally stable, is accompanied by oscillatory synchrony in the gamma range along a grouped contour, and is sensitive to both the contrast and length of contour inducers, thereby realizing the property of analog coherence in a network of spiking neurons.

Appendix

Model

First the mathematical equations for single cell dynamics are described, followed by network equations.

Hodgkin-Huxley dynamics and compartmental equations

Neurons are implemented as either one or two compartments governed by cable equations (Segev 1998). Compartmental membrane potential V is governed by an equation of the form:

$$C_m \frac{dV}{dt} = -\sum_k I_k, \tag{1}$$

where I_k refers to either of synaptic, axial, injected or membrane channel currents, as explained below. Membrane capacitance C_m is a function of compartment diameter (d) and length (l), and specific capacitance C_M:

$$C_m = \pi d l C_M . \tag{2}$$

In accordance with general practice, we set C_M=1μF/cm^2 (Koch 1999). Compartment dimensions d and l are the same for all neurons of a given layer. For clarity, dV/dt is noted dS/dt when the compartment is the soma, and by dD/dt when the compartment is a dendrite.

Somatic compartments are governed in part by Hodgkin-Huxley (1952) equations. To simplify notation, the collective influence of the leak, K^+, and Na^+ currents is denoted $f(S_i^j)$, where S_i^j stands for the somatic membrane potential of unit i in layer j:

$$f(S_i^j) = -g_L(S_i^j + |E_L|) - g_K n^4 (S_i^j + |E_K|) + g_{Na} m^3 h (E_{Na} - S_i^j), \tag{3}$$

where g_L, g_K and g_{Na} are the maximal conductances of the leak, K^+, and Na^+ channels respectively. E_L, E_K and E_{Na} represent the reverse potentials of the three respective currents, with specific values shown in Tables 3 and 4. The short form in (3) is not used for dendritic compartments since, for simplicity, the latter only have a passive leak current term $g_L(D_i^j + |E_L|)$. Gate variables n, m and h stand for the K^+ and Na^+ activating gates, and the Na^+ deactivating gate, respectively. The dynamical behavior of these gates is governed by the differential equation (where $k = \{n, m, h\}$):

$$\frac{dk}{dt} = \alpha_k(S_i^j)(1-k) - \beta_k(S_i^j)k. \tag{4}$$

The rate functions $\alpha_k(S_i^j)$ and $\beta_k(S_i^j)$ for the n, m and h gating variables are given in equations (5)-(7), respectively. The parameters for these equations were adapted from Traub and Miles (1991) such that cells transition to spiking through a supercritical Andronov-Hopf bifurcation (Izhikevich 2007) and have a stable attractor for small external input:

$$\alpha_n(V) = 0.032\frac{15-V}{\exp(\frac{15-V}{5})-1}$$

$$\beta_n(V) = 0.5\exp(\frac{-13.7-V}{40}), \tag{5}$$

$$\alpha_m(V) = 0.32\frac{13.0-V}{\exp(\frac{13-V}{4})-1}$$

$$\beta_m(V) = -0.28\frac{40-V}{\exp(\frac{40-V}{-5})-1}, \tag{6}$$

and

$$\alpha_h = 0.128\exp(\frac{17-V}{18})$$

$$\beta_h = \frac{4}{\exp(\frac{40-V}{5})+1}. \tag{7}$$

Setting $n(t)+h(t) \approx 0.84$ and $m = m_\infty(V)$, the (V,n)-phase plane (Izhikevich 2007) resulting from this choice of parameters is shown in Figure 13. It can be seen that, with these parameters, model neurons behave as threshold units, firing only for sufficiently depolarizing input.

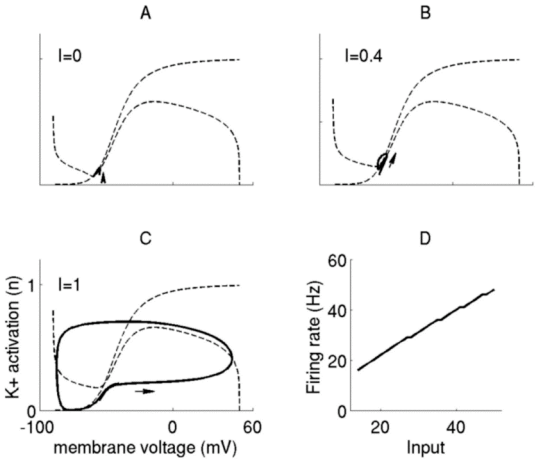

Fig. 13 (A)-(C) Parameters used for Hodgkin-Huxley equations allow model neurons to lose stability through a supercritical Andronov-Hopf bifurcation with increasing current input strength (*I*). The presence of a stable attractor at low *I* ensures limited outward propagation of signals in the bipole network. (D) These settings also render model neurons analog sensitive in terms of firing rate (Hz).

For inter-compartmental currents, the *actual* axial conductance of neurons within layer *j* is denoted q_j^c and is defined by:

$$q_j^c = \frac{\pi d_j^{c2}}{4 l_j^c R_j^A}. \tag{8}$$

Note that the diameter d_j^c and length l_j^c are the dimensions of the compartment *c* towards which the current appears to be directed in the relevant equation. Thus, *c* is replaced by *S* in the case of the soma and by *D* in the case of dendrite. Parameter R_j^A denotes specific axial resistance for neurons in layer *j*.

Synaptic input I_{ij}^{kl} from unit *i* of layer *k* to unit *j* of layer *l* is modeled by:

$$I_{ij}^{kl} = w_{ij}^{kl}\left(\sum_{t_n \in S_{ij}^{kl}} g_{ij}^{kl}(t-\delta_{ij}^{kl}, t_n) - \prod_{t_n \in S_{ij}^{kl}} g_{ij}^{kl}(t-\delta_{ij}^{kl}, t_n) \right), \tag{9}$$

where δ_{ij}^{kl} stands for axonal delay for that particular synaptic connection. Function $g_{ij}^{kl}(t-\delta_{ij}^{kl}, t_n)$ is a double exponential (e.g. Köhn and Wörgötter 1998):

$$g_{ij}^{kl}(t-\delta_{ij}^{kl}, t_n) = \begin{cases} \frac{p}{\tau_f - \tau_r}\left(e^{-\frac{t-\delta_{ij}^{kl}-t_n}{\tau_f}} - e^{-\frac{t-\delta_{ij}^{kl}-t_n}{\tau_r}}\right) & \tau_r \neq \tau_f \\ \frac{t}{\tau_r} e^{1-\frac{t-\delta_{ij}^{kl}-t_n}{\tau_r}} & \tau_r = \tau_f \end{cases}. \tag{10}$$

Constants τ_r and τ_f represent the rise-time and fall-time, respectively, of $g_{ij}^{kl}(t-\delta_{ij}^{kl}, t_n)$, which closely determines excitatory and inhibitory postsynaptic potentials (EPSP/IPSP) shape and duration (see Table 3). Constant *p* is set to ensure that $g_{ij}^{kl}(\cdot) \in [0\,1]$. The summation and multiplication in (9) are taken over the set S_{ij}^{kl} of the last two spike times t_n from unit *i* of layer *k* to unit *j* of layer *l*. Thus, keeping in mind that $g_{ij}^{kl}(\cdot) \in [0\,1]$, the multiplicative term ensures that the aggregated conductances remain between 0 and 1, which implies that synaptic current I_{ij}^{kl} varies between 0 and w_{ij}^{kl}. In the case of one-to-one connections, such that *i* = *j*, we abbreviate I_{ij}^{kl} by I_i^{kl} in equation (9).

The synaptic current resulting from the use of equation (9) is obtained by multiplying I_{ij}^{kl} with the voltage difference $(E - V_j^l)$. Here, V_j^l is the membrane voltage of the post-synaptic compartment of cell *j* in layer *l*, and E is the driving potential specific to the type of synapse under consideration. For excitatory connections, E is set to a depolarizing value (0 mV). For inhibitory connections, E is set to a hyperpolarizing value (-60 or -70 mV).

Network equations

The neural network is composed of 1-dimensional arrays of layer 4 and layer 2/3 pyramidal cells and *Left* and *Right* interneurons. Each of the four layers contains 51 neurons. Figure 2 illustrates a representative diagram of the network where layer 2/3 cells and interneurons span 7 spatial locations. External input is provided at each layer 4 pyramidal cell. Each layer 4 cell projects to a single layer 2/3 cell. Horizontal excitatory connections originating from layer 2/3 cell span a total of 7 spatial locations. *Left* interneurons receive such horizontal connections only from layer 2/3 cells on their left. The reverse holds for *Right* interneurons. *Left* and *Right* interneurons at a given spatial location inhibit each other via recurrent connections. Both interneurons also inhibit the layer 2/3 cell at the same spatial location. These connections are described more precisely below.

All network equations are written with endogenous currents (ionic channels, inter-compartmental) on the left-hand side and exogenous currents (synaptic, injections) on the right-hand side.

Layer 4 pyramidal cells

Each layer 4 pyramidal cell is modeled as a single compartment (a soma) S_i^4 that receives externally injected input X_i, where the latter is a scalar value for each neuron that is determined according to the simulation (see below):

$$C_m \frac{dS_i^4}{dt} - f(S_i^4) = X_i. \tag{11}$$

Layer 2/3 pyramidal cells

Each layer 2/3 pyramidal cell is composed of one soma (S_i^2) and one dendrite (D_i^2) compartment. The dendritic compartment receives bottom-up excitatory input from one layer 4 pyramidal cell (I_i^{42}) and recurrent excitatory input from a Gaussian neighborhood of layer 2/3 pyramidal cells ($\sum_{m=i-3}^{i+3} I_{mi}^{22}$):

$$C_m \frac{dD_i^2}{dt} - q_2^D(S_i^2 - D_i^2) + g_L(D_i^2 + |E_L|) = (E_{AMPA} - D_i^2)I_i^{42} + (E_{AMPA} - D_i^2)\sum_{m=i-3}^{i+3} I_{mi}^{22}. \tag{12}$$

The Gaussian distributed weight kernel and the axonal delay kernel implicit in I_{mi}^{22} are determined by equations (13) and (14), respectively:

$$w_{mi}^{kl} = g_{\max} e^{(m-i)^2/\sigma^2}, \tag{13}$$

$$\delta_{mi}^{kl} = 1 + 3 \cdot |i - m|, \tag{14}$$

where *m* and *i* are the indices of the pre- and post- synaptic units respectively, and σ=4.47. The maximal conductance, g_{max}, is specific to the projection and values used for it are in Table 3.

The somatic potential is defined as follows: Input from layer 2/3 pyramidal cells is significantly delayed in time, reflecting the presence of slow conduction delays in layer 2/3

horizontal connections. The soma receives convergent inhibitory input from the *Left* and *Right* interneurons at the same spatial location ($I_i^{L2} + I_i^{R2}$):

$$C_m \frac{dS_i^2}{dt} - q_2^S (D_i^2 - S_i^2) - f(S_i^2) = -(S_i^2 + |E_{GABA}|)[I_i^{L2} + I_i^{R2}]. \quad (15)$$

Equation (15) implies that inhibitory interneurons have a decisive effect on the layer 2/3 pyramidal cell they innervate due to their direct action on the soma.

Layer 2/3 inhibitory interneurons

Layer 2/3 interneurons are divided into two groups according to whether they are to the *Left* or to the *Right* of the layer 2/3 pyramidal cell they innervate. Since the form of the differential equations is similar and all parameters are the same, only equations for *Left* interneurons are explicitly given here. Each *Left* layer 2/3 interneuron is composed of one soma (S_i^L) and one dendrite (D_i^L) compartment. The dendritic compartment receives excitatory input from a half-Gaussian neighborhood of Layer 2/3 pyramidal cells located to its left ($\sum_{m=i-3}^{i-1} I_{mi}^{2L}$):

$$C_m \frac{dD_i^L}{dt} - q_L^D (S_i^L - D_i^L) + g_L (D_i^L + |E_L|) = (E_{AMPA} - D_i^L) \sum_{m=i-3}^{i-1} I_{mi}^{2L}. \quad (16)$$

The synaptic weight and axonal delay parameters that define I_{mi}^{2L} are determined by equations (13) and (14), respectively, with the additional constraint that it is set to 0 for $m>i$ in the case of *Left* interneurons and for $m<i$ in the case of *Right* interneurons.

Equation (17) governs the somatic membrane potential. The soma of a *Left* inhibitory interneuron only receives inhibitory input originating from the *Right* interneuron at the same spatial location:

$$C_m \frac{dS_i^L}{dt} - q_L^S (D_i^L - S_i^L) - f(S_i^L) = -(S_i^L + |E_{GABA}|) I_i^{RL}. \quad (17)$$

Local field potential (LFP) calculations

Local field potentials are calculated in the KinNeSS software package according to the methodology described in Versace et al. (2008). Emplacement of the electrode is determined by choosing a random location within [10-200]µm of the middle spatial location of the array of pyramidal layer 2/3 cells and aligning the electrode shank with the orientation of the cells. The distance of that electrode to the remaining 50 cells in the layer was uniformly random within the [10-1000]µm interval. The electrode is composed of five equally spaced electrode tips covering the entire length of layer 2/3 cells (i.e., sum of the dendrite and soma lengths). The LFP output did not differ significantly across electrode tips, so the respective outputs were averaged together in order to get a global estimate. The Fast Fourier Transform (FFT) was calculated on the averaged LFP thereby obtained.

Synchronization measure

The synchronization measure described in Rosenberg et al. (1989) was used to quantify the significance of the coupling in a selected pair of layer 2/3 pyramidal cells in Figure 9 (right

column). Each spike train is divided into L segments of length T. Let τ_j represent spikes times, then the finite Fourier transform of the l^{th} segment at frequency ω is given by:

$$d_N^T(\omega,l) = \sum_{(l-1)T \le \tau_j < lT} e^{-i\omega\tau_j}. \tag{18}$$

The cross-spectrum between two spike trains (denoted a and b) is further given by:

$$\hat{f}_{ab}(\omega) = \frac{1}{2\pi LT} \sum_{l=1}^{L} d_a^T(\omega,l)\overline{d_b^T(\omega,l)}, \tag{19}$$

where the bar indicates the complex conjugate. The squared magnitude of the estimated coherency between the two processes is defined as:

$$|R_{ab}(\omega)|^2 = \left| \frac{\hat{f}_{ab}(\omega)}{\hat{f}_{aa}(\omega)\hat{f}_{bb}(\omega)} \right|^2. \tag{20}$$

An upper 95% confidence limit to test for the presence of synchrony is given by $1-(0.05)^{1/(L-1)}$. This limit is plotted as a horizontal dashed line in Figure 9. Values above the line indicate significant coupling in the frequency range indicated on the x-axis. Here *L=50* and simulations were run for 25000ms, such that *T=500*ms, yielding a frequency resolution of 2Hz.

Parameters

Network

Biophysical parameters for synaptic connections and cells are given in Tables 3 and 4.

Table 4 Cell compartment dimensions, passive leak and axial conductivity parameters.

Population	Compartment	Diameter [mm]	Length [mm]	g_{leak} [mS/cm^2]	E_{leak} [mV]	Axial resistance [K·Ωcm]
4 pyr.	soma	0.001	0.005	0.01	-60	--
2/3 pyr.	soma	0.001	0.012	0.001	-60	--
	dendrite	0.001	0.032	0.005	-60	10
2/3 int.	soma	0.001	0.01	0.01	-60	--
	dendrite	0.001	0.007	0.005	-60	10

Weights and conduction delays

Horizontal weight kernels have a Gaussian shape as in equation (13) (half-Gaussian for connections reaching interneurons). The extent of the kernels is designed by dividing the maximum extent of horizontal connections by the width of a V1 hypercolumn (Yazdanbakhsh

and Grossberg 2004). Assuming a 7mm wide kernel and a 1mm wide hypercolumn, the kernel size is set to 7 spatial locations.

Horizontal axonal conduction delay kernels are linearly dependent on distance, as in equation (14). The delay between neighboring hypercolumns is calculated by dividing the hypercolumn width by horizontal conduction speed. Recent estimates of horizontal conduction speed in both monkey V1 and cat area 17 put it at approximately 0.3m/s (Bringuier et al. 1999; Girard et al. 2001; Hirsch et al. 1991). Using a hypercolumn width of 1mm, the conduction delay between neighboring hypercolumns is set to 3ms; see equation (14).

Simulation protocol

All simulations were performed with KinNeSS (Versace et al. 2008). Unless mentioned otherwise, firing rates are measured once the network reaches a steady state, by counting the number of spikes in the last second of simulation. An integration time-step of 0.05ms, 0.02ms, or 0.01ms was used to obtain numerically accurate results. All simulations took less than one hour on a dual 2Ghz AMD Opteron workstation with 4Gb of RAM running Linux. Unless mentioned otherwise, simulations were conducted for 2000ms of simulated time.

The results displayed in Figures 6, 8 and 9 represent averages (and standard deviation for error bars) from nine different parameter settings where the maximal conductance of AMPA connections were varied along two dimensions. Specifically, maximal conductance of the layer 4-2/3 connection was varied within the set {0.048, 0.049, 0.05} mS/cm^2 and maximal conductance of the layer 2/3-interneuron connection was varied within the set {0.036, 0.037, 0.038} mS/cm^2. Results appeared qualitatively similar in all cases. The simulations in Figure 7 correspond to the *middle* parameter configuration (i.e., values of 0.049 and 0.037 for respective parameters).

In simulations where this is relevant, stimulus contrast is defined as $X_i / 0.0006$, where X_i is the current injected into layer 4 pyramidal cells. Thus, nonlinearities between stimulus contrast and current input to cortical cells are not included in the simulations, implying that the simulations of contrast-dependent data may arise totally due to properties of the bipole network.

Simulation of latency to first spike (Figure 3D)

The results displayed in Figure 3D represents the difference between illusory and real contours in the latency of the first spike over the middle position of the contour, and for various current input strengths. Nonzero input was applied at locations 22 to 30 for real contours, whereas locations 25 to 27 were reset to zero for illusory contours. Current input was set to 0.0084, 0.015, 0.021, 0.03, 0.045, 0.06, 0.075, 0.09, 0.105 and 0.12nA.

Simulation of bipole property (Figure 5)

Nonzero input was applied to units at spatial locations 21, 22, 23, 29, 30 and 31 in the ID input array. Input strength at those locations was $X_i = 0.03$ nA. The simulation was conducted for 2000ms and firing rates were calculated by monitoring spikes in the last 500ms in order to ensure that the network has settled into a stable firing mode.

Short-range completion simulations (Figure 6)

Each stimulus bar is represented as an input (X_i) to a single location in Layer 4. This is motivated by considerations of recent estimates of the cortical magnification factor (cmf) at 4° of eccentricity (Polimeni et al. 2006). Accordingly, a cmf of 2.7mm/° gives approximately 1mm of cortical extent to a 30' stimulus bar as was used in the original study of Kapadia et al. (2000). However, 1-2mm is the approximate diameter of one hypercolumn. Thus, a single stimulus bar is presented to a single location. This is also consistent with their adjustment of the length of the bars to the size of the CRFs. Stimulus contrasts of 20, 30 and 50 percent were simulated by adjusting input strength to 0.012, 0.018 and 0.03 nA, respectively.

Simulations of long-range modulation (Figure 7)

The size of the bar stimuli in Polat et al. (1998) match CRF size which is here mapped to 3 adjacent columns. The distance between flanking bars is set to 7 locations, which is the shortest distance for which no inward completion occurred for the set of parameters considered. This particular constraint is in accordance with the method used in the original paper of Polat et al. (1998), and serves the purpose of studying long-range modulation instead of short-range completion. The current inputs simulated were (in nA): 0.0036, 0.006, 0.0072, 0.0126, 0.021, 0.03, 0.06, 0.09 and 0.12.

Outward propagation simulations (Figure 8)

In the original study of Crook et al. (2002), each stimulus bar was simulated as input to a single location. In the original study, the separation between the target cell recorded and the cell whose CRF receives the flanking stimulus was ~2mm. This corresponds to the approximate size of the cat's hypercolumn width (Lund 2003). Thus, in the simulations the target and flanking bars were presented at adjacent locations. The target input strength was set to 0.0096 nA and that of the flanker line was set to 0.06 nA in order to approach the 1-to-10 contrast ratio in the original study.

Horizontal summation simulations (Figure 9)

Arrays of collinear Gabor patches are represented by low contrast stimuli in the simulations. This is meant to represent the fact that the patches used in this study are of smaller diameter than the measured CRF size, such that they do not produce maximal activation. The length of stimuli used is determined by using the cmf (.21 mm/°) reported by the authors multiplied by the length (in degrees) of the original stimuli (here 5, 10, 15, 18, 23, 28 and 33 degrees). The corresponding array lengths are: 1, 2, 3, 4, 5, 6 and 7 mm, where each mm corresponds to one location in our simulations, which is in the order of the size of a hypercolumn in the tree shrew (Bosking 1997). For completeness, input stimuli are simulated at three contrast magnitudes by setting input strength to values of 0.0084, 0.0126 or 0.03 nA. The firing rate obtained is divided by the firing rate obtained for a 13-units long bar of high contrast (input strength set to 0.048 nA) simulated for the central parameter configuration in order to report quantities as relative activation with respect to a continuous bar of high contrast, consistent with the original study of Chisum et al. (2003).

Fast resynchronization simulations (Figure 10)

The simulations of Figure 10A and 10B were constructed by inserting a fixed random frame with input values ranging between 0 and 0.018 nA across spatial locations for the initial 100 ms and then switching to a homogeneous input stimulus for the remaining 900 ms. In the

case of the full contour simulation (Figure 10A), homogeneous input of magnitude 0.03 nA was applied to units 22 to 30. In the case of the illusory contour simulation (Figure 10B), the same homogeneous input was applied to units 22, 23, 24, 28, 29 and 30. Membrane potential traces of layer 2/3 bipole cells were low-pass filtered with a Butterworth filter of order 4 to remove single spikes but preserve slow oscillations, which simplifies detection of phase synchrony. Visual inspection of traces revealed that bursts occurred during ups and silent periods during troughs of the resulting filtered signals. The oscillations displayed therefore reliably represent burst occurrences.

Oscillatory synchrony simulations (Figure 11)

Simulations were run for 25000 ms. The full bar consisted of a 9-units wide stimulus. Separate bars consisted of 3-units wide stimuli, separated by a 3-units wide gap. The pair of cells selected for recording had their CRF located in the middle of each bar and were thus separated by 5 hypercolumns. This reflects the arrangement in the experimental recordings by Gray et al. (1989) where the pair of cortical cells was separated by approximately 7mm. Input strength was set to 0.03 nA. For the full bar and coherent bars condition, stimuli were presented with simultaneous injection in the layer 2/3 dendrites of 10ms sub-threshold white noise frames of amplitude varying in the interval [0 0.003] nA. For the incoherent bar condition, each short bar was presented for a randomly determined period of 300-500 ms. Each bar presentation was followed by a noise-only period of 300-500 ms, whose purpose was to attenuate the periodicity artificially induced in the delta band by the slow alternation of stimulus bars. Note that, exclusion of these periods from the simulation did not change the synchronization profile of Figure 11 (right) in the frequency bands of interest (mostly beta and gamma). Furthermore, the cross-correlograms reported in the middle column were shifted 100 ms in time to magnify the signal strength for the incoherent bar condition. Indeed, without this shift, the cross-correlogram output remains at 0 in the time frame considered for that condition, due to the inclusion of noise-only frames. However, the pattern of result remains the same when removing the shift. The coherence index $|R|^2$ was calculated according to equations (18)-(20).

LFP spectrum simulations (Figure 12)

Simulations were run for 25000 ms with 10 ms noise frames. Static input was set to 0.012 nA and time-varying noise magnitude spanned the interval [0 0.006] nA, such that the signal-to-noise ratio varied from 0 to 50%. The stimulus pattern simulated – i.e. a long bar, short bar, flankers-only bar, etc. – did not significantly affect the LFP power spectrum, whose peak varied in the upper 30 Hz to 50 Hz range. In the particular simulation shown in Figure 10, the stimulus pattern consisted of two 8 units wide flankers separated by a 5 units wide gap, and noise magnitude was set to 0 (no noise condition).

Threshold and analog sensitive single-cells (Figure 13)

The plots A, B and C were generated from equations (5)-(7) using the phase plane technique described in Izhikevich (2007), and for three representative current input levels (no current, low current, large depolarizing current). Plot D was generated by measuring the firing rate of a single neuron as the current input to that neuron was increased from 0 nA.

Funding
All authors were partially supported by CELEST, a National Science Foundation Science of Learning Center [SBE-0354378]; S.G. and M.V. were partially supported by the SyNAPSE program of the Defense Advanced Research Project Agency [HR001109-03-0001]; and S.G. and J.L. were also partially supported by the Defense Advanced Research Project Agency [HR001-09-C-0011].

References

Amir, Y., Harel, M., & Malach, R. (1993). Cortical hierarchy reflected in the organization of intrinsic connections in macaque monkey visual cortex. *Journal of Comparative Neurology, 334*, 19-46.

Anzai, A., Peng, X., & Van Essen, D.C. (2007). Neurons in monkey visual area V2 encode combinations of orientations. *Nature Neuroscience, 10*, 1313-1321.

Bar, M., Kassam, K.S., Ghuman, A.S., Boshyan, J., Schmidt, A.M., Dale, A.M., Hämäläinen, M.S., Marinkovic, K., Schacter, D.L., Rosen, B.R., & Halgren, E. (2006). Top-down facilitation of visual recognition. *Proceedings of the National Academy of Sciences, 103*, 449-454.

Berke J.D., Hetrick V., Breck J., & Green R.W. (2008). Transient 23- to 30-Hz oscillations in mouse hippocampus during exploration of novel environments. *Hippocampus, 18*, 519-529.

Blasdel, G.G., & Lund, J.S. (1983). Termination of afferent axons in macaque striate cortex. *Journal of Neuroscience, 3*, 1389-1413.

Bosking, W.H., Zhang, Y., Schofield, B., & Fitzpatrick, D. (1997). Orientation selectivity and the arrangement of horizontal connections in the tree shrew striate cortex. *Journal of Neuroscience, 17*, 2112-2127.

Boudreau, C.E., Williford, T.H., & Maunsell, H.R. (2006). Effects of task difficulty and target likelihood in area V4 of macaque monkeys. *Journal of Neurophysiology, 96*, 2377-2387.

Bringuier, V., Chavane, F., Glaeser, L., & Fregnac, Y. (1999). Horizontal propagation of visual activity in the synaptic integration field of area 17 neurons. *Science, 283*, 695-699.

Buffalo E.A., Fries P., & Desimone, R. (2004). Layer-specific attentional modulation in early visual areas. Program No. 717.6. 2004 Neuroscience Meeting Planner. San Diego, CA: Society for Neuroscience, 2004. Online. *Society for Neuroscience Abstracts, 30*, 717–716.

Bullier, J., Hupé, J.M., James, A., & Girard, P. (1996). Functional interactions between areas V1 and V2 in the monkey. *Journal of Physiology (Paris), 90*, 217-220.

Buschman T.J., & Miller E.K. (2008). Covert shifts in attention by frontal eye fields are synchronized to population oscillations. Submitted for publication.

Callaway, E.M., & Wiser, A.K. (1996). Contributions of individual layer 2-5 spiny neurons to local circuits in macaque primary visual cortex. *Visual Neuroscience, 13*, 907-922.

Cao, Y., & Grossberg, S. (2005). A laminar cortical model of stereopsis and 3D surface perception: Closure and da Vinci stereopsis. *Spatial Vision, 18*, 515-578.

Carpenter, G.A. (1979). Bursting phenomena in excitable membranes. *SIAM Journal of Applied Mathematics, 36*, 334-372.

Carpenter, G. & Grossberg, S. (1993). Normal and amnesic learning, recognition, and memory by a neural model of cortico-hippocampal interactions. *Trends in Neurosciences, 16*, 131-137.

Chisum, H.J., Mooser, F., & Fitzpatrick, D. (2003). Emergent properties of Layer 2/3 neurons reflect the collinear arrangement of horizontal connections in tree shrew visual cortex. *Journal of Neuroscience, 23*, 2947-2960.

Cohen, M.A., & Grossberg, S. (1984). Neural dynamics of brightness perception: Features, boundaries, diffusion, and resonance. *Perception & Psychophysics, 36*, 428-456.

Crook, J.M., Engelmann, R., & Löwel, S. (2002). GABA-inactivation attenuates collinear facilitation in cat primary visual cortex. *Experimental Brain Research, 143*, 295-302.

Domijan, D., Šetic, M. , & Švegar, D. (2007). A model of illusory contour formation based on dendritic computation. *Neurocomputing, 70*, 1977-1982.

Eckhorn, R., Bauer, R., Jordan, W., Brosch, M., Kruse, W., Munk, M., & Reitbock, H.J. (1988). Coherent oscillations: A mechanism of feature linking in the visual cortex? *Biological Cybernetics, 60*, 121-130.

Elston, G.N., Rosa, G.P., & Calford, M.B. (1996). Comparison of dendritic fields of Layer III pyramidal neurons in striate and extrastriate visual areas of the marmoset: A lucifer yellow intracellular injection study. *Cerebral Cortex, 6*, 807-813.

Ernst, U., Pawelzik, K., & Geisel, T. (1995). Synchronization induced by temporal delays in pulse-couple oscillators. *Physical Review Letters, 74*, 1570-1573.

Fang, L., & Grossberg, S. (2009). From stereogram to surface: How the brain sees the world in depth. *Spatial Vision, 22*, 45-82.

Ferster, D., Chung, S., & Wheat, H. (1996). Orientation selectivity of thalamic input to simple cells of cat visual cortex. *Nature, 380*, 249-252.

Field, D.J., Hayes, A., & Hess, R.F. (1993). Contour integration by the human visual system – evidence for a local association field. *Vision Research, 33*, 173-193.

Fitzhugh, R. (1955). Mathematical models of threshold phenomena in the nerve membrane. *Bulletin of Mathematical Biology, 17*, 252-278.

Fitzpatrick, D. (1996). The functional organization of local circuits in visual cortex: insights from the study of tree shrew striate cortex. *Cerebral Cortex, 6*, 329-341.

Francis, G., Grossberg, S., & Mingolla, E. (1994). Cortical dynamics of feature binding and reset: Control of visual persistence. *Vision Research, 34*, 1089-1104.

Fries, P., Reynolds, J.H., Rorie, A.E., & Desimone, R. (2001). Modulation of oscillatory neuronal synchronization by selective visual attention. *Science, 291*, 1560-1563.

Fukuda, T., Kosaka, T., Singer, W., & Galuske, R.A.W. (2006). Gap junctions among dendrites of cortical GABAergic neurons establish a dense and widespread intercolumnar network. *Journal of Neuroscience, 26*, 3434-3443.

Gautrais, J., & Thorpe, S. (1998). Rate coding versus temporal order coding: a theoretical approach. *Biosystems, 48*, 57-65.

Gerstner, W. (1996). Rapid phase locking in systems of pulse-coupled oscillators with delays. *Physical Review Letters, 76*, 1755-1758.

Gilbert, C.D., &Wiesel, T.N. (1983). Clustered intrinsic connections in cat visual cortex. *Journal of Neuroscience, 3*, 1116-1133.

Girard, P., Hupé, J.M., & Bullier, J. (2001). Feedforward and feedback connections between areas V1 and V2 of the monkey have similar rapid conduction velocities. *Journal of Neurophysiology, 85*, 1328-1331.

Golubitsky M., & Stewart, I. (2006). Nonlinear dynamics of networks: the groupoid formalism. *Bulletin of the American Mathematical Society, 43*, 305-364.

Gray, C.M., König, P., Engel, A.K., & Singer, W. (1989). Oscillatory responses in cat visual cortex exhibit inter-columnar synchronization which reflects global stimulus properties. *Nature, 338*, 334-337.

Gray, C.M., & Singer, W. (1989). Stimulus-specific neuronal oscillations in orientation columns of cat visual cortex. *Proceedings of the National Academy of Sciences USA, 86*, 1698-1702.

Gregoriou, G.G., Gotts, S.J., Zhou, H., & Desimone, R. (2009). High-frequency, long-range coupling between prefrontal and visual cortex during attention. *Science, 324*, 1207-1210.

Grossberg, S. (1973). Contour enhancement, short term memory, and constancies in reverberating neural networks. *Studies in Applied Mathematics, 52*, 217-257. Reprinted in *Studies of Mind and Brain*, S. Grossberg (1982). D. Reidel Publishing Company: Dordrecht, Holland.

Grossberg. S. (1976a). Adaptive pattern classification and universal recoding, I: Parallel development and coding of neural feature detectors. *Biological Cybernetics, 23*, 121-134.

Grossberg, S. (1976b). Adaptive pattern classification and universal recoding, II: Feedback, expectation, olfaction, and illusions. *Biological Cybernetics, 23*, 187-202.

Grossberg, S. (1980). How does a brain build a cognitive code?. *Psychological Review, 87*, 1-51.

Grossberg, S. (1984). Outline of a theory of brightness, color, and form perception. In E. Degreef and J. van Buggenhaut (Eds.). *Trends in mathematical psychology* (pp. 59-85). Amsterdam: North-Holland.

Grossberg, S. (1999). How does the cerebral cortex work? Learning, attention, and grouping by the laminar circuits of visual cortex. *Spatial Vision, 12*, 163-185.

Grossberg, S. (2003). How does the cerebral cortex work? Development, learning, attention, and 3D vision by laminar circuits of visual cortex. *Behavioral and Cognitive Neuroscience Reviews, 2*, 47-76.

Grossberg, S. (2007). Consciousness CLEARS the mind. *Neural Networks, 20*, 1040-1053.

Grossberg, S. (2009). Beta oscillations and hippocampal place cell learning during exploration of novel environments. *Hippocampus*, in press.

Grossberg, S., & Grunewald, A. (1997). Cortical synchronization and perceptual framing. *Journal of Cognitive Neuroscience, 9*, 117-132.

Grossberg, S., & Mingolla, E. (1985a). Neural dynamics of perceptual grouping: Textures, boundaries, and emergent segmentations. *Perception & Psychophysics*, 38, 141-171.

Grossberg, S., & Mingolla, E. (1985b). Neural dynamics of form perception: Boundary completion, illusory figures, and neon color spreading. *Psychological Review, 92*, 173-211.

Grossberg, S., Mingolla, E., & Ross, W.D. (1997). Visual brain and visual perception: how does the cortex do perceptual grouping? *Trends in Neuroscience, 20*, 106-111.

Grossberg, S., & Raizada, R.D.S. (2000). Contrast-sensitive perceptual grouping and object-based attention in the laminar circuits of primary visual cortex, *Vision Research, 40*, 1413-1432.

Grossberg, S., & Somers, D. (1991). Synchronized oscillations during cooperative feature linking in a cortical model of visual perception. *Neural Networks, 4*, 453-466.

Grossberg, S., & Swaminathan, G. (2004). A laminar cortical model of 3D perception of slanted and curved surfaces and of 2D images: development, attention and bistability. *Vision Research, 44*, 1147-1187.

Grossberg, S., & Todorović, D. (1988). Neural dynamics of 1-D and 2-D brightness perception: A unified model of classical and recent phenomena. *Perception & Psychophysics, 43*, 241-277.

Grossberg, S., & Versace, M. (2008). Spikes, synchrony, and attentive learning by laminar thalamocortical circuits. *Brain Research, 1218*, 278-312.

Grossberg, S., & Williamson, J.R. (2001). A neural model of how horizontal and interlaminar connections of visual cortex develop into adult circuits that carry out perceptual grouping and learning. *Cerebral Cortex, 11*, 37-58.

Grossberg, S., & Yazdanbakhsh, A. (2005). Laminar cortical dynamics of 3D surface perception: Stratification, transparency, and neon color spreading. *Vision Research, 45*, 1725-1743.

Grossberg, S., Yazdanbakhsh, A., Cao, Y., & Swaminathan, G. (2008). How does binocular rivalry emerge from cortical mechanisms of 3-D vision? *Vision Research, 48*, 2232-2250.

Guttman, S. and Sekuler, A., & Kellman, P.J. (2003). Temporal variations in visual completion: A reflection of spatial limits? *Journal of Experimental Psychology. Human perception and performance, 29*, 1211-1227.

Halgren, E., Mendola, J., Chong, C.D.R., & Dale, A.M. (2003). Cortical activation to illusory shapes as measured with magnetoencephalography. *Neuroimage, 18*, 1001-1009.

Heeger, D.J. (1992). Normalization of cell responses in cat striate cortex. *Visual Neuroscience, 9*, 181-197.

Hirsch, J.A., & Gilbert, C.D. (1991). Synaptic physiology of horizontal connections in the cat's visual cortex. *Journal of Neuroscience, 11*, 1800-1809.

Hochstein, S., & Ahissar, M. (2002). View from the top: Hierarchies and reverse hierarchies in the visual system. *Neuron, 36*, 791-804.

Hodgkin, A.L., & Huxley, A.F. (1952). A quantitative description of membrane current and its application to conduction and excitation in nerve. *Journal of Physiology, 117*, 500-544.

Holmgren, C., Harkany, T., Svennenfors, B., & Zilberter, Y. (2003). Pyramidal cell communication within local networks in layer 2/3 of rat neocortex. *Journal of Physiology, 551*, 139-153.

Hupé, J.-M., James, A.C., Girard, P., Lomber, S.G., Payne, B.R., & Bullier, J. (2001). Feedback connections act on the early part of the responses in monkey visual cortex. *Journal of Neurophysiology, 85*, 134-145.

Izhikevich, E. (2007). *Dynamical systems in neuroscience*. Cambridge: MIT Press.

Kapadia, M., Westheimer, G., & Gilbert, C.D. (2000). Spatial distribution of contextual interactions in primary visual cortex and in visual perception. *Journal of Neurophysiology, 84*, 2048-2062.

Kellman, P.J., & Shipley, T.F. (1991). A theory of visual interpolation in object perception. *Cognitive Psychology, 23*, 141-221.

Kisvárday, Z.F., Tóth, É., Rausch, M, & Eysel, U.T. (1997). Orientation-specific relationship between populations of excitatory and inhibitory lateral connections in the visual cortex of the cat. *Cerebral Cortex, 7*, 605-618.

Koch, C. (1999). *Biophysics of computation: information processing in single neurons*. New York: Oxford University Press.

Köhn, J., & Wörgötter, F. (1998). Employing the Z-transform to optimize the calculation of the synaptic conductance of NMDA and other synaptic channels in network simulations. *Neural Computation, 10*, 1639-1651.

Lamme, V.A.F., Rodriguez-Rodriguez, V., & Spekreijse, H. (1999). Separate processing dynamics for texture elements, boundaries and surfaces in primary visual cortex of the macaque monkey. *Cerebral Cortex, 9*, 406-413.

Lamme, V.A.F., & Roelfsema, P.R. (2000). The distinct modes of vision offered by feedforward and recurrent processing. *Trends in Neuroscience, 23*, 571-579.

Lesher, G.W., & Mingolla, E. (1993). The role of edges and line-ends in illusory contour formation. *Vision Research, 33*, 2253-2270.

Levitt, J.B., Yoshioka, T., & Lund, J.S. (1994). Intrinsic cortical connections in macaque visual area V2: evidence for interaction between different functional streams. *Journal of Comparative Neurology, 342*, 551-570.

Li, Z. (1998). A neural model of contour integration in the primary visual cortex. *Neural Computation, 10*, 903-940.

Lund, J.S., Angelucci, A., & Bressloff, P.C. (2003). Anatomical substrates for functional columns in macaque monkey primary visual cortex. *Cerebral Cortex, 12*, 15-24.

Lund, J.S., Griffiths, S., Rumberger, A., & Levitt, J.B. (2001). Inhibitory synapse cover on the somata of excitatory neurons in macaque monkey visual cortex. *Cerebral Cortex, 11*, 783-795.

McGuire, B.A., Gilbert, C.D., Rivlin, P.K., & Wiesel, T.N. (1991). Targets of horizontal connections in macaque primary visual cortex. *Journal of Comparative Neurology, 305*, 370-392.

Megías, M., Emri, Z., Freund, T.F., & Gulyás, A.I. (2001). Total number and distribution of inhibitory and excitatory synapses on hippocampal CA1 pyramidal cells. *Neuroscience, 102*, 527-540.

Meyer, G., & Ming, C. (1988). The visible persistence of illusory contours. *Canadian Journal of Psychology, 42*, 479-488.

Milner, P.A. (1974). A model for visual shape recognition. *Psychological Review, 81*, 5221-525.

Murray, R.F., Sekuler, A.B., & Bennett, P.J. (2001). Time course of amodal completion revealed by a shape discrimination task. *Psychonomics Bulletin & Review, 8*, 713-720.

Murray, M.M., Wylie, G.R., Higgins, B.A., Javitt, D.C., Schroeder, C.E., & Foxe, J.J. (2002). The spatiotemporal dynamics of illusory contour processing: combined high-density electrical mapping, source analysis, and functional magnetic resonance imaging. *Journal of Neuroscience, 22*, 5055-5073.

Oram, M.W., Perrett, D.I. (1992). Time course of neural responses discriminating different views of the face and head. *Journal of Neurophysiology, 68*, 70-84.

Peterhans, E., & Von Der Heydt, R. (1989). Mechanisms of contour perception in monkey visual cortex II. Contour bridging gaps. *Journal of Neuroscience, 9*, 1749-1763.

Polat. U., Mizobe, K., Pettet, M.W., Kasamatsu, T., & Norcia, A.M. (1998). Collinear stimuli regulate visual responses depending on cell's contrast threshold. *Nature, 391*, 580-584.

Polimeni, J., Balasubramanian, M., & Schwartz, E.L. (2006). Multi-area visuotopic map complexes in macaque striate and extra-striate cortex. *Vision Research, 46*, 3336-3359.

Polsky, A., Mel, B.W., & Schiller, J. (2004). Computational subunits in thin dendrites of pyramidal cells. *Nature Neuroscience, 7*, 621-627.

Raizada, R.D.S., & Grossberg, S. (2001). Context-sensitive bindings by the laminar circuits of V1 and V2: A unified model of perceptual grouping, attention and orientation contrast. *Visual Cognition, 8*, 431-466.

Ringach, D.L., & Shapley, R. (1996). Spatial and temporal properties of illusory contours and amodal boundary completion. *Vision Research, 36*, 3037-3050.

Rosenberg, J.R., Amjad, A.M., Breeze, P., Brillinger, D.R., & Halliday, D.M. (1989). The Fourier approach to the identification of functional coupling between neuronal spike trains. *Progress in Biophysics and Molecular Biology, 53*, 1-31.

Salin, P., & Bullier, J. (1995). Corticocortical connections in the visual system: structure and function. *Physiological Reviews, 75*, 107-154.

Samonds, J.M., Zhou, Z., Bernard, M.R., & Bonds, A.B. (2006). Synchronous activity in visual cortex encodes collinear and cocircular contours. *Journal of Neurophysiology, 95*, 2602-2616.

Sandell, J.H., & Schiller, P.H. (1982). Effect of cooling area 18 on striate cortex cells in the squirrel monkey. *Journal of Neurophysiology, 48*, 38-48.

Sarpeshkar, R. (1998). Analog Versus Digital: Extrapolating from electronics to neurobiology. *Neural Computation, 10*, 1601-1638.

Schmidt, K.E., Goebel, R. Löwel, S., & Singer, W. (1997). The perceptual grouping criterion of colinearity is reflected by anisotropies of connections in the primary visual cortex. *European Journal of Neuroscience, 9*, 1083-1089.

Segev, I. (1998). Cable and Compartmental Models of Dendritic Trees. In J.M. Bower and D. Beeman, *The book of genesis*. New York: Springer-Verlag/TELOS.

Sekuler, A.B., & Palmer, S.E. (1992). Perception of partly occluded objects: A microgenetic analysis. *Journal of Experimental Psychology: General, 121*, 95-111.

Shmuel, A., Korman, M., Sterkin, A., Harel, M., Ullman, S., Malach, R., & Grinvald, A. (2005). Retinotopic axis specificity and selective clustering of feedback projections from V2 to V1 in the Owl monkey. *Journal of Neuroscience, 23*, 2117-2131.

Silito, A.N., Jones, H.E. Gerstein, G.L., & West, D.C. (1994). Feature-linked synchronization of thalamic relay cell firing induced by feedback from the visual cortex. *Nature, 369*, 479-482.

Soriano, M., Spillmann, L., Bach, M. (1996). The abutting grating illusion. *Vision Research, 36*, 109-116.

Spruston, N. (2008). Pyramidal neurons: dendritic structure and synaptic integration. *Nature Reviews Neuroscience, 9*, 206-221.

Stetter, D.D., Das, A., Bennett, J., & Gilbert, C.D. (2002). Lateral connectivity and contextual interactions in macaque primary visual cortex. *Neuron, 36*, 739-750.

Tallon, C., Bertrand, O., Bouchet, P., & Pernier, J. (1995). Gamma-range activity evoked by coherent visual stimuli in humans. *European Journal of Neuroscience, 7*, 1285-1291.

Tamas, G., Somogyi, P., & Buhl, E.H. (1998). Differentially interconnected networks of GABAergic interneurons in the visual cortex of the cat. *Journal of Neuroscience, 18*, 4255-4270.

Thomson, A.M., & Bannister, A.P. (2003). Interlaminar connections in the neocortex. *Cerebral Cortex, 13*, 5-14.

Thorpe. S., Delorme, A., & Van Rullen, R. (2001). Spike-based strategies for rapid processing. *Neural Networks, 14*, 715-725.

Traub, R.D., & Miles, R. (1991). *Neuronal networks of the hippocampus*. Cambridge: Cambridge University Press.

Tusa, R.J., Rosenquist, A.C., & Palmer, L.A. (1979). Retinotopic organization of areas 18 and 19 in the cat. *Journal of Comparative Neurology, 185*, 657-678.

VanRullen, R., Delorme, A., & Thorpe, S.J. (2001). Feed-forward contour integration in primary visual cortex based on asynchronous spike propagation. *Neurocomputing, 38-40*, 1-4.

VanRullen, R., Guyonneau, P., & Thorpe. S.J. (2005). Spike times make sense. *Trends in Neuroscience, 28*, 1-4.

Versace, M., Ames, H., Léveillé, J., Fortenberry, B., Mhatre, H., & Gorchetchnikov, A. (2008). KInNeSS: A modular framework for computational neuroscience. *Neuroinformatics, 6*, 291-309.

von der Heydt, R., Peterhans, E., & Baumgartner, G. (1984). Illusory contours and cortical neuron responses. *Science, 224*, 1260-1262.

von der Malsburg, C. (1981). The correlation theory of brain function. Internal Report 81-2, Dept. of Neurobiology, Max-Planck Institute for Biophysical Chemistry, Göttingen, Germany.

Yazdanbakhsh, A., & Grossberg, S. (2004). Fast synchronization of perceptual grouping in laminar visual cortical circuits. *Neural Networks*, 17, 707-718.

Yen, S.-C., & Finkel, L.H. (1998). Extraction of perceptually salient contours by striate cortical networks. *Vision Research, 38*, 719-741.

Yen, S.-C., Menschik, E.D., & Finkel, L.H. (1999). Perceptual grouping in striate cortical networks mediated by synchronization and desynchronization. *Neurocomputing, 26-27*, 609-616.

Yoshino, A., Kawamoto, M., Yoshida, T., Kobayashi, N., Shigemura, J., Takahashi, Y., & Nomura, S. (2006). Activation time course of responses to illusory contours and salient region: a high-density electrical mapping comparison. *Brain Research, 1071*, 137-144.